

Practical limitations on robustness and scalability of quantum Internet

Abhishek Sadhu,^{1,2,*} Meghana Ayyala Somayajula,³ Karol Horodecki,^{4,5,†} and Siddhartha Das^{2,‡}

¹*Raman Research Institute, Bengaluru, Karnataka 560080, India*

²*Center for Security, Theory and Algorithmic Research,
International Institute of Information Technology,
Hyderabad, Gachibowli, Telangana 500032, India*

³*Department of Computer Science Engineering, G Narayanamma
Institute of Technology and Science, Hyderabad, Telangana 500104, India*

⁴*Institute of Informatics, National Quantum Information Centre,
Faculty of Mathematics, Physics and Informatics,
University of Gdańsk, Wita Stwosza 57, 80-308 Gdańsk, Poland*

⁵*International Centre for Theory of Quantum Technologies,
University of Gdańsk, Wita Stwosza 63, 80-308 Gdańsk, Poland*

(Dated: August 25, 2023)

As quantum theory allows for information processing and computing tasks that otherwise are not possible with classical systems, there is a need and use of quantum Internet beyond existing network systems. At the same time, the realization of a desirably functional quantum Internet is hindered by fundamental and practical challenges such as high loss during transmission of quantum systems, decoherence due to interaction with the environment, fragility of quantum states, etc. We study the implications of these constraints by analyzing the limitations on the scaling and robustness of the quantum Internet. Considering quantum networks, we present practical bottlenecks for secure communication, delegated computing, and resource distribution among end nodes. Motivated by the power of abstraction in graph theory (in association with quantum information theory), that allows us to consider the topology of a network of users spatially separated over long distances around the globe or separated as nodes within a small space over a processor or circuit within a same framework, we consider graph-theoretic quantifiers to assess network robustness and provide critical values of communication lines for viable communication over quantum Internet.

In particular, we begin by discussing limitations on usefulness of isotropic states as device-independent quantum key repeaters which otherwise could be useful for device-independent quantum key distribution. We consider some quantum networks of practical interest, ranging from satellite-based networks connecting far-off spatial locations to currently available quantum processor architectures within computers, and analyze their robustness to perform quantum information processing tasks. Some of these tasks form primitives for delegated quantum computing, e.g., entanglement distribution and quantum teleportation, that are desirable for all scale of quantum networks, be it quantum processors or quantum Internet. For some examples of quantum networks, we also present algorithms to perform different quantum network tasks of interest such as constructing the network structure, finding the shortest path between a pair of end nodes, and optimizing the flow of resources at a node.

CONTENTS

		Critical time and length scales for repeater networks	9
I. Introduction	2	Limitations on quantum network topologies	10
II. Preliminaries	3	C. Robustness measure for networks	11
III. Limitations on the network architecture with repeaters	4	D. Comparison of the robustness of network topologies	12
		E. Critical nodes in a network	13
IV. Graph Theoretic analysis of networks	6	V. Real World Instances	14
A. Graph theoretic framework of networks	6	A. Entanglement distribution between cities	14
B. Limitations on repeater networks	8	B. Quantum Processors	16
Critical success probability for repeater networks	8	C. Network propositions	18
		VI. Algorithms	19
		A. Shortest path between a pair of nodes	19
		B. Network Construction	20
		C. Identifying the critical nodes	20
		D. Resource allocation at a node	21

* abhisheks@rri.res.in

† karol.horodecki@ug.edu.pl

‡ das.seed@iiit.ac.in

VII. Discussion	21
Acknowledgments	22
A. Dual rail encoding of photons	22
B. Two-qubit states	22
C. Two qubit Bell measurement on isotropic states	23
D. Actions of some quantum channels	23
1. The qubit depolarizing channel	23
2. The erasure channel	24
3. The qubit thermal channel	24
E. The atmospheric channel	25
F. Entanglement distribution across cities	26
G. Limitations of linear repeater networks	26
H. Sparsity index of a star network	27
I. Analysis of time-varying quantum networks	28
References	29

I. INTRODUCTION

The quantum Internet [1–3] is a network of users who are enabled to perform desired quantum information processing and computing tasks among them. Some of the important communication and computing tasks that we envision to be possible in full-fledged quantum Internet are cryptographic tasks against quantum adversaries of varying degree [4–13], quantum computation [14–21], distributed quantum computing [22–27], delegated quantum computing [28–31], quantum sensing [32–38], quantum clock synchronization [39–41], quantum communication [19, 42–53], superdense coding [42, 45, 54, 55], quantum teleportation [56–60], randomness generation and distribution [61–65], etc. Some of the crucial primitives for many of the quantum information and computing tasks are the distribution of resources like entanglement [13, 19, 66–73], nonlocal quantum correlations [19, 74–83], or quantum coherence [84–87], etc.

Recent technological advancements have made it possible to realise quantum networks with fewer users at small distances [88–91], however, the short lifetime of physical qubits (in some coherent states or quantum correlations) [92–95], the high loss experienced during the distribution of quantum systems across different channels [13, 96–100] and the use of imperfect measurement devices [11, 101–104] limits the realization of quantum networks for practical purposes. It is important to study the limitations of the quantum Internet, be it network connecting nodes in a quantum processor (or quantum

computer) or network connecting users in different spatial locations to allow quantum information processing tasks among them. In this work, we use tools and techniques from graph (network) theory and quantum information theory to shed light on the limitations on the robustness and scalability of the quantum Internet.

Unlike classical signals, the losses associated with the transmission of quantum states between two parties via a lossy channel cannot be reduced by using amplifiers since the measurement will disturb the system [105] and unknown quantum states cannot be cloned [106]. An alternative approach is to use quantum repeaters [101, 107, 108] to enable entanglement distribution [3, 69, 109, 110] and perform cryptographic tasks [13, 111–115] over lossy channels. The quantum repeater-based protocols use entanglement swapping [116–119] and optionally entanglement purification [43, 120, 121] at intermediate points along the quantum channel. Advances in satellite-based quantum communication networks [97, 122–124], improving system designs [125–128], and developing post-processing techniques [129–133] are considerable efforts towards overcoming constraints on realizing the quantum Internet.

If we focus on the topology of the quantum Internet, certain important questions arise: What is the effective structure of the underlying network to enable different parties to perform information processing tasks? Once a network structure is established, a significant concern is regarding its susceptibility to node and edge failures. A resilient network should possess the ability to carry out different information-processing tasks even if a substantial portion of its nodes becomes inactive. Consequently, it is desirable that the realization of the quantum Internet withstands the failure of a fraction of its nodes and edges. This naturally leads to the question of how to evaluate the resilience of the quantum Internet and identify the nodes that are most crucial to its overall functioning. Having designed robust networks to enable different parties to perform desired information processing tasks, it is important to ask what strategies can be employed to optimize the flow of resources at the buffer nodes.

The power of abstraction in graph (network) theory [134, 135] that provides a general formalism to analyze networks without getting into specific details of implementation [136], motivates the use of graph-theoretic tools in analyzing the scalability and robustness of a global scale quantum Internet. Focusing on the robustness of networks, we present link sparsity, sparsity index and critical parameter as figures of merit for comparing different network topologies. We also apply ideas from percolation theory [137, 138] to discuss the robustness of networks formed when performing a class of information processing tasks over any lattice network (sufficiently large graph). Considering the currently available quantum processors [139–142] as real-world instances of graphical networks, we observe that the 54-qubit square topology of the Sycamore processor developed by Google [139] has the highest node connection

strength and the lowest link sparsity. With the possibility of having a 1024-qubit quantum processor in the future, we extend the 54-qubit layout to include 1024 qubits and present its figures of merit.

The information-processing tasks that will be implemented using the quantum Internet will determine its structure. The building blocks for the structure of any network are the elementary links connecting two nodes of the network. It is therefore important to assess the limitations at the elementary link scale. To do this, we consider a network where the nodes share an isotropic state. We present the critical success probability of the elementary links for performing different tasks. Extending to a more general network, we present a trade-off between the channel length and time spent at the nodes such that the state shared by the end nodes remains useful for different tasks.

There is a strong motivation to enable remote places to securely access quantum processors via the quantum Internet and perform delegated quantum computing [28–30] over the quantum Internet as it is less resource extensive on the individual user. To illustrate this, we may assume an instance where a user with limited computing resources in Bangalore requests to securely access the IBM Quantum Hub at Poznań [143] via the quantum Internet. Enabling secure access requires the sharing of entangled states among distant nodes [69, 73, 144–148] along with performing secure cryptographic tasks against adversaries. We present limitations involved in implementing these tasks. In particular, we present limitations on using isotropic state [149] for distilling secret keys via DI-QKD protocols [5, 6] over the quantum Internet. We provide upper bounds on the number of elementary links between the end nodes for performing secure communication and information-processing tasks. Considering a satellite-based network for distributing entangled states between far-off cities, we present bottlenecks on its implementation.

The satellite-based network can be used in the future to share entangled states between different airports across the globe to aid in secure communication between them. We present the figures of merit of a global mesh network having 3462 nodes and 25482 edges connecting the major airports in the world along with its entanglement yield considering currently available and desirable technology available in the future. On a local scale, the quantum Internet can be used for secure communication between a central agency and end parties. It may be desirable here for the central agency to prevent direct communication between the end parties. We consider a fiber-based star network for this task and present bottlenecks in its implementation.

To implement secure communication and share entanglement between the end nodes there are certain underlying network tasks that are needed to be performed. We present algorithms for implementing the network tasks. An important task is constructing the network structure to connect groups of network nodes. Once we obtain the

network structure, we need the network path connecting two end nodes to enable the sharing of resources among them. In a general network, buffer nodes connecting multiple input and output channels may be present. The input channels may request to store resources at the buffer nodes while the output channels may request to extract resources stored in it. It is required to have a strategy to allocate resources to and from the buffer nodes in the network. We provide algorithms to perform these network tasks.

The structure of the paper is as follows. We introduce notations and review basic concepts and standard definitions in Sec. II. In Sec. III, we present limitations on using isotropic states in networks for device-independent secret key distillation. We present an upper bound on the number of elementary links between the end nodes such that the state shared by them remains entangled and is useful for different information-processing tasks. In Sec. IV, we present graph theoretic quantifiers to assess and compare network robustness. We provide critical values of network parameters for implementing different tasks over the quantum Internet. In Sec. V, we present limitations on the potential uses of the quantum Internet for real-world applications. In particular, we present practical bottlenecks in the distribution of entangled states between far-off cities using a satellite-based network in Sec. V A. Considering different quantum processor architectures as networks, we observe their figures of merit in Sec. V B. In Sec. V C, we first consider the task of connecting major airports across the globe via the satellite-based network and present the yield of the network. Then we present practical bottlenecks in connecting a central agency to the end parties via a star-based network. In Sec. VI, we present algorithms that are primitives for implementing different information-processing tasks using the quantum Internet. In particular, we consider the tasks of finding the shortest network path between a pair of nodes, resource allocation at a node with multiple input and output channels and constructing the network structure for connecting different end nodes. We provide concluding remarks in Sec. VII.

II. PRELIMINARIES

In this section, we introduce notations and review basic concepts and standard definitions that will be used frequently in later sections. We consider quantum systems associated with the separable Hilbert spaces. The Hilbert space of a quantum system A and a composite system AB are denoted as \mathcal{H}_A and $\mathcal{H}_{AB} := \mathcal{H}_A \otimes \mathcal{H}_B$ respectively. Let the dimension of the Hilbert space \mathcal{H}_A be denoted as $|A| := \dim(\mathcal{H}_A)$. A quantum state of A is represented by the density operator defined on \mathcal{H}_A . The density operator ρ defined on \mathcal{H} satisfies three necessary conditions: (i) $\rho \geq 0$, (ii) $\rho = \rho^\dagger$, (iii) $\text{Tr}[\rho] = 1$. A pure state is a rank-one density operator given by $\psi_A := |\psi\rangle\langle\psi|_A$ where $|\psi\rangle_A \in \mathcal{H}_A$. The set of density op-

erators of A is denoted by $\mathcal{D}(\mathcal{H}_A)$. We denote the density operator of a composite system AB as $\rho_{AB} \in \mathcal{D}(\mathcal{H}_{AB})$; $\text{Tr}_B[\rho_{AB}] = \rho_A \in \mathcal{D}(\mathcal{H}_A)$ is the reduced state of A . Separable states are those that can be expressed as a convex combination of product states

$$\rho_{AB} = \sum_x p_x \rho_A^x \otimes \rho_B^x, \quad (1)$$

where $p_x \in [0, 1]$ and $\sum_x p_x = 1$. States that cannot be expressed in the form of Eq. (1) are said to be entangled. A maximally entangled state of bipartite system AB is defined as $\Psi_{AB}^+ := |\Psi^+\rangle\langle\Psi^+|_{AB}$ where

$$|\Psi^+\rangle_{AB} = \frac{1}{\sqrt{d}} \sum_{i=0}^{d-1} |ii\rangle_{AB}, \quad (2)$$

$d = \min\{|A|, |B|\}$ is the Schmidt-rank of the state Ψ_{AB}^+ , and $\{|i\rangle\}_{i=0}^{d-1}$ forms an orthonormal set of vectors (kets). We next discuss families of states called isotropic states and Werner states.

Definition 1. (*Isotropic state [149]*) An isotropic state $\rho_{AB}^I(p, d)$ is $U \otimes U^*$ invariant for any arbitrary unitary U . For $p \in [0, 1]$, such a state can be written as

$$\rho_{AB}^I(p, d) := p\Psi_{AB}^+ + (1-p)\frac{\mathbb{1}_{AB} - \Psi_{AB}^+}{d^2 - 1} \quad (3)$$

where Ψ_{AB}^+ is a maximally entangled state of Schmidt rank d . An Isotropic state $\rho_{AB}^I(p, d)$ written as in Eq. (3) is separable iff $p \in [0, 1/d]$.

Remark 1. We can also express isotropic states (Eq. (3)) as

$$\rho_{AB}^I(p(\lambda), d) = \lambda\Psi_{AB}^+ + (1-\lambda)\frac{\mathbb{1}_{AB}}{d^2} \quad (4)$$

for $p(\lambda) = [\lambda(d^2 - 1) + 1]/d^2$ and $\lambda \in [-1/(d^2 - 1), 1]$. We note that $\lambda^n \geq 0$ for all even $n \in \mathbb{N}$. For our purposes in this work, we will be restricting $\rho_{AB}^I(p(\lambda), d)$ to the case $\lambda \in [0, 1]$ without loss of generality. We call λ as the visibility of the state $\rho_{AB}^I(p(\lambda), d)$.

Definition 2. (*Werner state [150]*) A Werner state $\rho_{AB}^W(p, d)$ is $U \otimes U$ invariant for any arbitrary unitary U . For $p \in [0, 1]$, such a state can be written as

$$\rho_{AB}^W(p, d) := p\frac{2}{d(d+1)}\Pi_{AB}^+ + (1-p)\frac{2}{d(d-1)}\Pi_{AB}^- \quad (5)$$

where $\Pi_{AB}^\pm := (\mathbb{I} \pm F_{AB})/2$ are the projections onto the symmetric and anti-symmetric sub-spaces of \mathcal{H}_A and \mathcal{H}_B . $F_{AB} = \sum_{ij} |i\rangle\langle j|_A \otimes |j\rangle\langle i|_B$ is the SWAP operator on A and B . A Werner state $\rho_{AB}^W(p, d)$ written as in Eq. (5) is separable iff $p \in [1/2, 1]$.

A quantum channel $\mathcal{M}_{A \rightarrow B} : \mathcal{D}(\mathcal{H}_A) \rightarrow \mathcal{D}(\mathcal{H}_B)$ is a completely positive, trace-preserving map. A measurement channel $\mathcal{M}_{A' \rightarrow AX}$ is a quantum instrument whose action is defined as

$$\mathcal{M}_{A' \rightarrow AX}(\cdot) := \sum_x \mathcal{E}_{A' \rightarrow A}^x(\cdot) \otimes |x\rangle\langle x|_X, \quad (6)$$

where each $\mathcal{E}_{A' \rightarrow A}^x$ is a completely positive, trace nonincreasing map such that $\mathcal{M}_{A' \rightarrow AX}$ is a quantum channel and X is a classical register that stores the measurement outcomes. A classical register X is represented by a set of orthogonal quantum states $\{|x\rangle\langle x|_X\}$ defined on the Hilbert space \mathcal{H}_X . We define qubit Bell measurement with success probability q as

$$\mathcal{M}_{A_1 A_2 \rightarrow X}(\cdot) := q \sum_{j=1}^4 \text{Tr}[\Psi^{(j)}(\cdot) \Psi^{(j)}] |j\rangle\langle j|_X + (1-q) \text{Tr}[\cdot] \otimes |\perp\rangle\langle\perp|_X, \quad (7)$$

where $\{\Psi_{A_1 A_2}^{(j)}\}_{j=1}^4$ denotes projective measurements on the set of maximally entangled states $\{\Psi_{A_1 A_2}^+, \Psi_{A_1 A_2}^-, \Phi_{A_1 A_2}^+, \Phi_{A_1 A_2}^-\}$ (see Appendix B for details) and $|\perp\rangle \perp |j\rangle$.

Definition 3. (*Max-heap data structure [151]*) A max heap is a tree-based data structure that satisfies the following heap property: for any given node Y , if X is a parent of Y , then the key (the value) of X is greater than or equal to the key of Y .

In Fig. 1, we present the tree and array representations of a max heap data structure with 9 nodes.

In the bipartite Bell scenario where there are two observables $\{x_1, x_2\}$ for Alice and $\{y_1, y_2\}$ for Bob, the family of tilted CHSH operators introduced in [63] is given by

$$I_\alpha^\beta := \beta x_1 + \alpha x_1 y_1 + \alpha x_1 y_2 + x_2 y_1 - x_2 y_2, \quad (8)$$

where $\alpha \geq 1$ and $\beta \geq 0$. The choice of $\beta = 0$ and $\alpha = 1$ corresponds to the CHSH operator [75]. The local upper bound of the tilted CHSH operator is given by $\beta + 2\alpha$. The quantum upper bound of the tilted CHSH operator is given by $2\sqrt{(1 + \alpha^2)(1 + \frac{\beta^2}{4})}$.

Note 1. In general, the logarithmic function can have base as the natural exponent e or some natural number greater than or equal to 2. In this paper, we consider the logarithmic function \log to have base 2 and natural logarithm \ln to have base e unless stated otherwise.

III. LIMITATIONS ON THE NETWORK ARCHITECTURE WITH REPEATERS

A method for perfectly secure communication between a receiver and a sender requires sharing cryptographic keys between the parties [4]. The secret keys can be

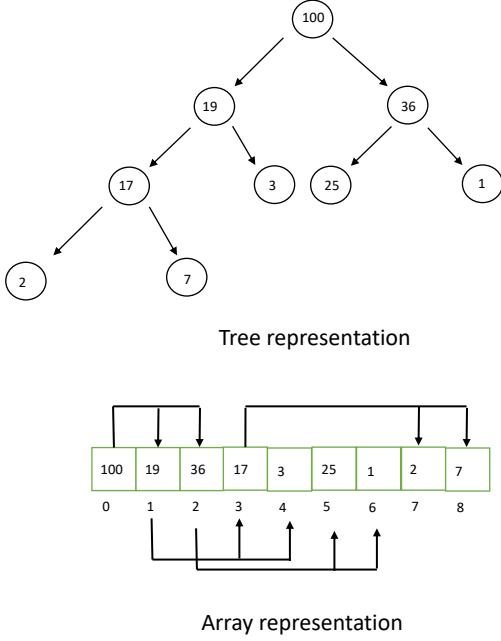


FIG. 1: In this figure, we present the tree and array representations of a max-heap data structure with 9 nodes. In the tree representation, the nodes are shown in circles with the node values written inside them. In the array representation, the nodes are stored in continuous memory allocations (shown in green boxes numbered 0 to 9). The relation between the nodes is shown using arrows. We see that it satisfies the heap property: the value (or key) of a parent is always greater than its children. (Color online)

shared between the receiver and the sender using quantum key distribution (QKD) protocols. For these protocols, the transmission of quantum states from one party to another is an important step. However, the transmission of quantum states from a sender to a receiver via a lossy channel inevitably degrades the state being transmitted. The overlap of the shared state with the intended state typically decreases monotonically with the length of the channel. Unlike a classical signal, for quantum states this loss cannot be reduced using amplifiers since the measurement will disturb the system [105] and also quantum states cannot be cloned [106]. The degradation of the quantum states when transmitted over a quantum channel places limitations on the distance over which there can be secure communication [13]. This limitation may be overcome by using entanglement-based QKD protocols [5, 152] along with quantum repeaters [101, 153, 154].

In classical computing, there is a strong motivation to use delegated computation in the form of cloud computing as it is less resource extensive on the individual user. Now, given that there is no full clarity regarding the path

along which quantum computing will develop, delegated quantum computing [28–30] is a vision ahead [155]. This vision has been supported by efforts to provide access to quantum processors over the Internet [156]. The recent developments in the field of QKD and the current high-speed global communication networks only increase the scope for early adoption of delegated quantum computing.

Let us consider the task of sharing secret key between two distant parties over a repeater-based network. Let the parties say Alice and Bob each have two-qubit isotropic states given by $\rho_{AA'}^I(p(\lambda), 2)$ and $\rho_{BB'}^I(p(\lambda), 2)$ respectively and $\lambda \in [0, 1]$. Alice and Bob send halves of their isotropic states to a repeater station. The repeater station performs a Bell measurement on the halves of the isotropic states with success probability q . The action of the Bell measurement is described by Eq. (C2) (see Appendix C for details.) Assuming that error correction is possible post-Bell measurement, then from a single use of the repeater Alice and Bob with a probability q share the two-qubit isotropic state

$$\rho_{AB}^I(p(\lambda^2), 2) = \lambda^2 \Psi_{AB}^+ + \frac{1}{4}(1 - \lambda^2) \mathbb{1}_{AB} \quad (9)$$

of visibility λ^2 and q being the success probability of performing the successful Bell measurement by the repeater station. The state $\rho_{AB}^I(p(\lambda^2), 2)$ is separable if $\lambda \leq 1/\sqrt{3}$. All two-qubit states are entanglement distillable if and only if they are entangled [157]. All entanglement distillable states have non-zero rates for secret-key distillation [158]. Alice and Bob can use the shared state $\rho_{AB}^I(p(\lambda^2), 2)$ to perform a DI-QKD protocol based on the tilted CHSH inequality [63] or the modified standard CHSH inequality [159]. It was shown in [160] that for such protocols, the device-independent secret key distillation rate is zero when the visibility λ^2 of isotropic state $\rho_{AB}^I(p(\lambda^2), 2)$ is below the critical threshold

$$\gamma_{\text{crit}}^\theta = \frac{\gamma_L^\theta + 1}{3 - \gamma_L^\theta}, \quad (10)$$

where $\gamma_L^\theta = 1/(\cos \theta + \sin \theta)$ and $\theta \in (0, \pi/2)$. The standard CHSH-based DI-QKD protocols use settings with $\theta = \pi/4$, which gives $\gamma_{\text{crit}}^{\pi/4} \approx 0.7445$. The DI-QKD rate is known to be non-zero for $\lambda^2 \geq 0.858$ [6]. For n repeater stations in between them, Alice and Bob with probability q^n share the two-qubit isotropic state

$$\rho_{AB}^I(p(\lambda^{n+1}), 2) = \lambda^{n+1} \Psi_{AB}^+ + \frac{1}{4}(1 - \lambda^{n+1}) \mathbb{1}_{AB} \quad (11)$$

of visibility λ^{n+1} and q being the success probability of performing a Bell measurement by the individual repeater stations.

Proposition 1. *Consider the repeater relay network where the neighbouring nodes v_i and v_j share a two-qubit isotropic state $\rho_{ij}^I(p(\lambda^2), 2)$. The end nodes of such*

a network share the state $\rho_{AB}^I(p(\lambda^{n+1}), 2)$ of visibility λ^{n+1} with probability q^n . For $\lambda \in ((\gamma_{\text{crit}}^\theta)^{1/n+1}, \sqrt{\gamma_{\text{crit}}^\theta})$, device-independent secret key distillation rate is zero among the end nodes even though neighbouring nodes can distill device-independent secret keys at non-zero rate.

Proof. The end nodes can use the shared state $\rho_{AB}^I(p(\lambda^{n+1}), 2)$ to perform a DI-QKD protocol based on the tilted CHSH inequality [63] or the modified standard CHSH inequality [159]. The device-independent secret key rate for such protocols becomes zero for $\lambda^{n+1} \in (0, \gamma_{\text{crit}}^\theta)$. This limits λ to the range

$$\lambda \in (0, (\gamma_{\text{crit}}^\theta)^{1/(n+1)}) \quad (12)$$

when no secret key can be distilled. Also for the neighbouring nodes v_i and v_j , the key rate is zero for

$$\lambda \in (0, \sqrt{\gamma_{\text{crit}}^\theta}). \quad (13)$$

It follows from Eq. (12) and (13) that for λ in the range $((\gamma_{\text{crit}}^\theta)^{1/n+1}, \sqrt{\gamma_{\text{crit}}^\theta})$ the device-independent secret key distillation rate is zero for the end nodes even though neighbouring nodes can distill secret keys at non-zero rates. \square

For non-zero key rates from tilted CHSH inequality-based and the modified standard CHSH inequality-based DI-QKD protocols we require

$$n < \lfloor \frac{\log(1/\gamma_{\text{crit}}^\theta)}{\log(1/\lambda)} - 1 \rfloor, \quad (14)$$

where $\lfloor \cdot \rfloor$ denotes the floor function. For values of n below the above threshold, we will have secure keys with a probability q^n . We plot in Fig. 2, the dependence of n on λ for performing DI-QKD protocol with non-zero key rate based on the tilted and modified standard CHSH inequality. In the plot, we have set $\gamma_{\text{crit}}^\theta$ to be 0.7445. In Fig. 2, we observe that the neighbouring nodes of a repeater chain network sharing a two-qubit isotropic state $\rho_{AB}^I(p(\lambda^2), 2)$ with high visibility allows a large number of repeater stations between the end nodes for performing a DI-QKD protocol with non-zero key rates. However, the success probability of the DI-QKD protocol decreases with the increase in the number of repeater stations. In the bipartite scenario with two binary inputs and two binary outputs, there is a region where the device is non-local but has zero key [161]. Results similar to Proposition 1 and Eq. (14) would apply to such a scenario if considered appropriately.

We present in Appendix G bounds on the number of repeater stations such that the state shared by the end nodes of the network is useful for different information processing tasks. The repeater network discussed in this section can be generalised to a network structure with multiple pairs of end nodes.

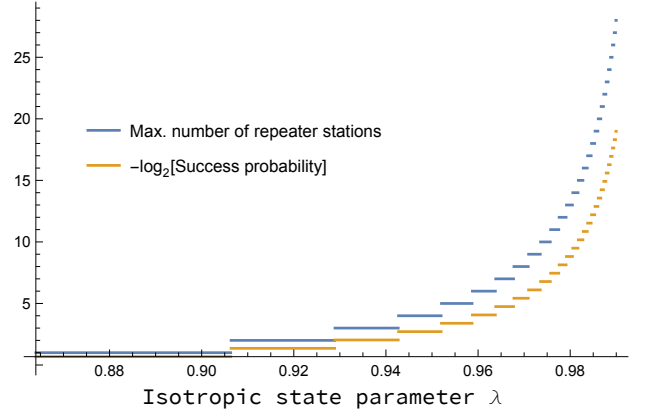


FIG. 2: In this figure, we plot the allowed number of repeater stations and the success probability of performing a DI-QKD protocol with non-zero key rates by Alice and Bob as a function of the isotropic state parameter λ when the critical threshold from Eq. (10) is $\gamma_{\text{crit}}^\theta = 0.7445$. (Color online)

Graph theory provides a framework to assess the topology of networks having spatially separated users across the globe, as well as networks with nodes within a small space over a processor or circuit without getting into specific details of implementation. Motivated by the power of abstraction, in the following section, we analyze the robustness and scalability of the quantum Internet using graph theoretic tools.

IV. GRAPH THEORETIC ANALYSIS OF NETWORKS

In this section, we first present a graph theoretic framework for networks. Using such a framework, we analyze the limitations on the scalability of repeater-based networks for different information processing tasks. Looking into the robustness of network topologies, we present tools for measuring network robustness and identifying the critical components. Using such measures, we compare the robustness of different network topologies.

A. Graph theoretic framework of networks

Let us consider networks represented as graph $G(\mathbb{V}, \mathbb{E})$ classified as weighted and undirected. A graph is a mathematical structure that is used to define pairwise relations between objects called nodes. Let \mathbb{V} denote the set of nodes, also called vertices and \mathbb{E} denotes the set of edges which are pairs of nodes of the graph that connect the vertices. Let us denote $|\mathbb{V}|$ as N_v and $|\mathbb{E}|$ as N_e , where $|\mathbb{X}|$ denotes the size of the set \mathbb{X} . Let us denote the vertices of the graph G as $v_i \in \mathbb{V}$ and the edges connecting the nodes $\{v_i, v_j\} \in \mathbb{V}$ as $e_{ij} \in \mathbb{E}$. We denote the path connecting two distant nodes v_i and v_k as $\mathcal{P}(v_i, v_k)$ having length

$\text{len}(\mathcal{P})$. The shortest network path between v_i and v_k is denoted as $\text{dist}(v_i, v_k)$. We call the shortest path length between the most distant nodes of the graph the diameter of the graph. A value $w_{ij} \in \mathbb{R}$ assigned to an edge e_{ij} of the graph is called the edge weight. The graph G together with w_{ij} is called a weighted graph. A graph where the edges do not have a direction is called an undirected graph. The edges of an undirected graph indicate a bidirectional relationship where each edge can be traversed from both directions.

In general, the nodes, edges, and edge weights of a network can change with time (see Appendix I for details). In this work, we will deal with undirected, weighted graphs depicting networks for communication tasks among multiple users. The edges in the graph are representative of links in the corresponding network, where links between nodes are formed due to quantum channels (or gates) over which resources are being transmitted between connected nodes. We denote labelled graphs as $G(\mathbb{V}, \mathbb{E}, \mathbb{L})$ where \mathbb{L} denotes the set of labels associated with the vertices and edges of the graph.

We denote the nodes of the graph that are present between the end nodes when traversing along a path from one end node to another as the virtual nodes associated with the path. We note that while analysing the network for different tasks, it may be possible that all the virtual nodes of the network are secure and cooperate in the execution of the task. We call this the cooperating strategy. It may also be possible that some virtual nodes of the network may be compromised and are not available for the task. We call this the non-cooperating strategy.

Definition 4. Let a network depicted by an undirected, weighted graph $G(\mathbb{V}, \mathbb{E})$, where $v_i \in \mathbb{V}$ for $i \in [N_v]$, be given by $\mathcal{N}(G(\mathbb{V}, \mathbb{E}))$. The success probability of transmitting a desirable resource χ between any two different nodes v_i, v_j (i.e., when $i \neq j$) connected with edge e_{ij} is given by p_{ij} ; we assume $p_{ii} = 1$ for an edge e_{ii} connecting a node v_i with itself. The weight $w(e_{ij})$ for each edge e_{ij} is given by $-\log p_{ij}$. We define an effective weight $w_*(e_{ij})$ of an edge e_{ij} over which the resource χ is transmitted between v_i to v_j for a particular information processing task (Task $_*$) as, for all $i, j \in [N_v]$

$$w_*(e_{ij}) := \begin{cases} -\log p_{ij} & \text{if } p_{ij} \geq p_*, \\ \infty & \text{otherwise,} \end{cases} \quad (15)$$

where p_* is the critical probability below which the desired information processing task Task $_*$ fails. Since $G(\mathbb{V}, \mathbb{E})$ is undirected, we have $p_{ij} = p_{ji}$, $w(e_{ij}) = w(e_{ji})$, $w_*(e_{ij}) = w_*(e_{ji})$.

Observation 1. The weight $w(e_{ij})$ for an edge is path-dependent and additive across connecting edges. If a resource χ is being transmitted between nodes v_i and v_l by traversing the virtual nodes v_j and v_k in an order $v_i \rightarrow v_j \rightarrow v_k \rightarrow v_l$, i.e., through a connecting path $e_{ij} \rightarrow e_{jk} \rightarrow e_{kl}$, then the weight $w(e_{i \rightarrow j \rightarrow k \rightarrow l}) = w(e_{ij}) + w(e_{jk}) + w(e_{kl}) = -\log p_{ij} p_{jk} p_{kl}$. The effective

weight $w_*(e_{ij})$ is also path-dependent. The effective weight $w_*(e_{i \rightarrow j \rightarrow k \rightarrow l}) = w_*(e_{ij}) + w_*(e_{jk}) + w_*(e_{kl}) = -\log p_{ij} p_{jk} p_{kl}$ if $p_{ij} p_{jk} p_{kl} \geq p_*$, else $w_*(e_{i \rightarrow j \rightarrow k \rightarrow l}) = \infty$. If any of the p_{ij}, p_{jk}, p_{kl} is strictly less than p_* then $p_{ij} p_{jk} p_{kl} < p_*$. To maximize the success probability of transmitting the resource χ between any two nodes of the network, it is desirable to select the path between these two nodes that has the minimum weight.

Definition 5 (Critically large network). We define a network $\mathcal{N}_{\text{crit}}(G(\mathbb{V}, \mathbb{E}))$ as critically large network for the Task $_*$ if

$$\forall_{e_{ij} \in \mathbb{E}} p_{ij} \leq c, \text{ where } c \in (0, 1), \quad (16)$$

and it contains least two vertices $x_0, y_0 \in \mathbb{V}$ which are at distance

$$\text{dist}(x_0, y_0) \geq \left\lceil \frac{\log p_*}{\log c} \right\rceil + 1, \quad (17)$$

where p_* is the critical probability for successful transmission of resource χ (Definition 4).

Proposition 2. Assume that it is possible to perform Task $_*$ between any two distinct nodes v_i, v_j of the network $\mathcal{N}_{\text{crit}}(G(\mathbb{V}, \mathbb{E}))$ if and only if nodes v_i, v_j can share resource χ over the network path $\mathcal{P}(v_i, v_j)$ having success probability $s(\mathcal{P}(v_i, v_j)) \geq p_* > 0$. Then

$$\begin{aligned} \exists_{n_0 < \infty} \forall_{\{v_i, v_j\} \in \mathbb{V}} & \left[\text{dist}(v_i, v_j) \geq n_0 \right. \\ & \Rightarrow \forall_{\mathcal{P}(v_i, v_j)} s(\mathcal{P}(v_i, v_j)) < p_* \left. \right] \quad (18) \end{aligned}$$

In other words, there will be at least two vertices in this network, that cannot share resource χ by Task $_*$.

Proof. We begin with an observation that the success probability of sharing a resource between vertices $\{v_i, v_j\}$ along the path $\mathcal{P}(v_i, v_j)$ is given by $s(\mathcal{P}(v_i, v_j)) := p_{ik} \dots p_{mj}$. The vertices v_i and v_j cannot share a resource along the path $\mathcal{P}(v_i, v_j)$ if $s(\mathcal{P}(v_i, v_j)) < p_*$.

Let us choose n_0 such that $c^{n_0} < p_*$. Consider now any two vertices v_i and v_j be such that $\text{dist}(v_i, v_j) > n_0$ (we note that the set of such vertices is non-empty since $\text{dist}(x_0, y_0) > n_0$ by assumption in Eq. (17)). Then any path $\mathcal{P}(v_i, v_j)$ has length $l \geq \text{dist}(v_i, v_j)$. The success probability of sharing resource along the path $\mathcal{P}(v_i, v_j)$ is given by $s(\mathcal{P}(v_i, v_j)) = p_{ik} p_{kl} \dots p_{mj} \leq (\max\{p_{ik}, p_{kl}, \dots, p_{mj}\})^l \leq c^l \leq c^{n_0} < p_*$. Thus for any $\{v_i, v_j\}$ at distance $\geq n_0$, there does not exist a path $\mathcal{P}(v_i, v_j)$ with $s(\mathcal{P}(v_i, v_j)) \geq p_*$. \square

Consider a d -dimensional lattice $G_{\text{lat}}(\mathbb{V}, \mathbb{E})$ having $|\mathbb{V}| \rightarrow \infty$. The vertex set \mathbb{V} is defined as the set of elements of \mathbb{R}^d with integer coordinates. Let us denote $G_{\text{sg}}(\mathbb{V}_{\text{sg}}, \mathbb{E}_{\text{sg}})$ as a finite subgraph of $G(\mathbb{V}, \mathbb{E})$ from which the entire graph can be constructed by repetition and

$$\exists_{N_{\text{sg}} \ll |\mathbb{V}|} : \forall_{v_j \in \mathbb{V}_{\text{sg}}} \text{degree}(v_j) \leq N_{\text{sg}}. \quad (19)$$

A percolation configuration $\omega_p = (\omega_{ij} : e_{ij} \in \mathbb{E})$ on the graph $G(\mathbb{V}, \mathbb{E})$ is an element of $\{0, 1\}^{|\mathbb{E}|}$. If $\omega_{ij} = 1$, the edge is called open, else closed. A configuration ω_p is a subgraph of $G(\mathbb{V}, \mathbb{E})$ with vertex set \mathbb{V} and edge-set $\mathbb{E}_p := \{e_{ij} \in \mathbb{E} : \omega_{ij} = 1\}$ (cf. [162]).

Theorem 1. *Let us consider performing Task* (Definition 4) over the lattice $G_{lat}(\mathbb{V}, \mathbb{E})$ where each edge is open with probability p_{ij} and $0 < p_* \leq p_{ij} < 1$. Then the network arising among nodes from this task does not form a percolation configuration, i.e., a connected component of length N_c such that $N_c/|\mathbb{V}| > 0$.*

The above theorem follows from the facts that there are periodic repetitions of the finite subgraph $G_{sg}(\mathbb{V}_{sg}, \mathbb{E}_{sg})$ in $G_{lat}(\mathbb{V}, \mathbb{E})$ and there exists at least two subgraphs whose distance is greater than critical threshold for inter-subgraph nodes to remain connected for Task* (see Proposition 2). See also [138, Page 20] for discussion on 1-dimensional lattice and condition for percolation to exist.

Definition 6. *Consider a network $\mathcal{N}(G(\mathbb{V}, \mathbb{E}))$ with $|\mathbb{V}| = N_v$ and $w(e_{ij})_{i,j}$. The adjacency matrix \mathbf{A} of the network is a $N_v \times N_v$ matrix such that for all $i, j \in [N_v]$ we have*

$$[\mathbf{A}]_{ij} = w(e_{ij}), \quad (20)$$

and the effective adjacency matrix \mathbf{A}_* of the network is given by

$$[\mathbf{A}_*]_{ij} = w_*(e_{ij}). \quad (21)$$

The effective success matrix of any network $\mathcal{N}(G(\mathbb{V}, \mathbb{E}))$ for the transmission of a desirable resource χ (associated with Task*) between its nodes is an $N_v \times N_v$ matrix \mathbf{U}_* such that for all $i, j \in [N_v]$ we have

$$[\mathbf{U}_*]_{ij} := \begin{cases} p_{ij}^{\max} & \text{if } p_{ij}^{\max} \geq p_* \text{ for } i \neq j, \\ 0 & \text{otherwise,} \end{cases} \quad (22)$$

where p_{ij}^{\max} is the maximum success probability of transmitting the desirable resource χ between nodes v_i and v_j over all possible paths between the two nodes.

The elements $[\mathbf{U}_*]_{ij}$ of the success matrix provide the highest probability with which χ can be shared between the nodes v_i and v_j thus corresponds to the path having minimum cumulative effective weight. Let us consider a graph of diameter 2 as shown in Fig. 3. The adjacency matrix and the success matrix for this graph are different as $[\mathbf{A}]_{14} = [\mathbf{U}_*]_{14} = 0.79$ while $[\mathbf{A}]_{12} = 0.198$ and $[\mathbf{U}_*]_{12} = 0.54173$. We observe that the success probability of transferring χ between nodes v_1 and v_2 via a non-cooperating strategy leads to a lower success probability $p_{1 \rightarrow 2}$ as compared to that via a cooperative strategy $p_{1 \rightarrow 3 \rightarrow 2}$.

Note 2. *Henceforth, we will be dealing with communication over networks where the success probability of trans-*

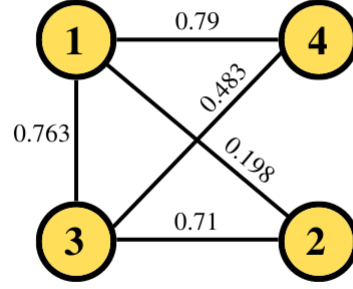


FIG. 3: A partially connected mesh network with 4 nodes. In this graph the adjacency matrix \mathbf{A} and the success matrix \mathbf{U} are different. While performing an information processing task using this network say transferring a resource χ from $v_1 \rightarrow v_2$, it is preferable to use a cooperative strategy $v_1 \rightarrow v_3 \rightarrow v_2$ over a non-cooperative strategy $v_1 \rightarrow v_2$ as it has a higher success probability. (Color online)

mitting resources from a node a to node c via node b is less than or equal to the multiplication of the success probability of resource transmission from a to b and b to c .

B. Limitations on repeater networks

In this subsection, we present the critical success probability of the elementary links for implementing different information processing tasks. Extending to a linear repeater-based network, we present the critical time and length scales for implementing different information processing tasks.

Critical success probability for repeater networks

Consider a network $\mathcal{N}(G(\mathbb{V}, \mathbb{E}))$ for performing a particular information processing task denoted by the symbol Task*. As examples, we let the Task* be sharing of entanglement, or implementing teleportation protocol between the nodes $\{v_i, v_j\} \in \mathbb{V}$. Let v_i, v_j share an isotropic state given by

$$\rho_{ij}^I(p, d) = p_{ij} \Psi_{ij}^+ + (1 - p_{ij}) \frac{\mathbb{1}_{ij} - \Psi_{ij}^+}{d^2 - 1}, \quad (23)$$

via a qudit depolarising channel (cf. [13, 100]). Following Eq. (15), let us denote p_* as the critical success probability below which the task Task* fails. The quantum state

shared by nodes v_i and v_j become separable for $p_{ij} < 1/d$, this implies a critical success probability $p_*^{\text{ent}} \geq 1/d$. The singlet fraction of the state shared between v_i and v_j is given by $f_{ij} = p$. The maximum achievable teleportation fidelity of a bipartite $d \times d$ system in the standard teleportation scheme is given by $F = \frac{f_{ij}d+1}{d+1}$ [163]. The maximum fidelity achievable classically is given by $F_{cl} = \frac{2}{d+1}$. Thus the shared state between v_i and v_j is useful for quantum teleportation if $f_{ij} > 1/d$. The critical success probability p_*^{tel} for performing teleportation protocol over $\mathcal{N}(G(\mathbb{V}, \mathbb{E}))$ is $p_*^{\text{tel}} \geq 1/d$, where $p_* = 1/d$ can be taken in an ideal situation.

Critical time and length scales for repeater networks

Consider an entanglement swapping-based repeater network. Let there be two sources S_1 and S_2 producing dual-rail encoded entangled pairs (for details see Appendix A) in the state Ψ^+ with probability η_s and with probability $1-\eta_s$ produces a vacuum state. The source S_1 sends one qubit from its entangled pair to Alice and the other to the repeater station via optical fibers of length l . Similarly, S_2 sends one qubit from its entangled pair to Bob and the other to the repeater station via optical fibers of length l . Let the qubits be stored in quantum memories at the repeater station and the stations of Alice and Bob for time t . We model the evolution of the qubits through the fiber and at the quantum memory as a qubit erasure channel (see Sec. D 2) with channel parameter $\eta_e = e^{-(\alpha l + \beta t)}$, where α and β are respectively the properties of the fiber and the quantum memory. The repeater station performs a Bell measurement on its share of qubits with success probability q . After the repeater station has performed the Bell measurement, Alice and Bob share the state Ψ^+ with probability $q \eta_s^2 e^{-2(\alpha l + \beta t)}$ (cf. [13, Eq. (64)]). Let p_* be the critical probability below which the shared state becomes useless for some information processing tasks, we then require

$$q \eta_s^2 e^{-2(\alpha l + \beta t)} > p_*. \quad (24)$$

We observe that Eq. (24) bounds the length of the optical fibers and the time till which the qubits can be stored in the quantum memories. This motivates the definition of the critical length of the fibers l_c and the critical storage time at the nodes t_c above which the shared state becomes useless for information processing tasks. These two critical parameters are related via the expression

$$\alpha l_c + \beta t_c < \frac{1}{2} \ln \left(\frac{q \eta_s^2}{p_*} \right). \quad (25)$$

We plot in Fig. 4 the critical fibre length l_c and the critical storage time t_c for different qubit architectures and set $p_* = 0.5$ for some desired Task*.

Let us introduce a finite number of repeater stations between the two end nodes, each performing Bell mea-

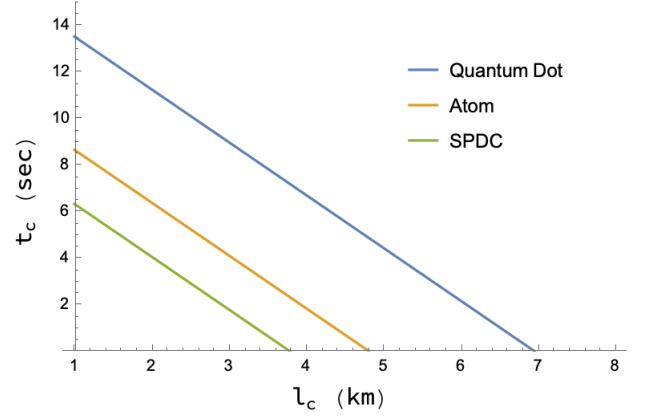


FIG. 4: In this figure, we consider a repeater-based network and plot the critical storage time t_{cr} as a function of critical fiber length l_{cr} for different qubit architectures. The single photon architectures have efficiencies (a) $\eta_s = 0.97$ (Quantum Dots [164]) (b) $\eta_s = 0.88$ (Atoms [165]) and (c) $\eta_s = 0.84$ (SPDC [166]). We set $p_* = 0.5$, $q = 1$, $\alpha = 1/22 \text{ km}^{-1}$ and $\beta = 1/50 \text{ sec}^{-1}$. (Color online)

surements on its share of qubits. The network is useful for Task* when

$$q^r \eta_s^{r+1} e^{-2r(\alpha l + \beta t)} > p_*, \quad (26)$$

where r denotes the number of repeater stations between the end nodes. Let l_{cr} and t_{cr} denote the critical length of the fiber and the critical storage time of the quantum memory. These two critical parameters are then related via the expression

$$\alpha l_{cr} + \beta t_{cr} < \frac{1}{2r} \ln \left(\frac{q^r \eta_s^{r+1}}{p_*} \right). \quad (27)$$

We plot in Fig. 5 the critical fiber length l_{cr} and the critical storage time t_{cr} such that Eq. (27) holds for different values of r . The bounds on l_{cr} and t_{cr} for other values of r not shown in Fig. 5 can be obtained from Eq. (27). We observe that for a given information processing task, increasing the number of repeater stations allows shorter fiber lengths and quantum memory storage times.

We note that the optimal rate of two-way assisted quantum communication or entanglement transmission (i.e., in an informal way, it is the maximum number of ebits per use of the channel in the asymptotic limit of the number of uses of the channel) over an erasure channel, also called LOCC (local operations and classical communication)-assisted quantum capacity of an erasure channel, is given by $\eta_e \log_2 d$ [167], where $1 - \eta_e$ is the erasing probability and d is the dimension of the input Hilbert space. Two-way assisted quantum and private capacities for erasure channel coincide [168, 169] (see [170] for strong-converse capacity). Two-way assisted private and quantum capacities for a qubit erasure channel is

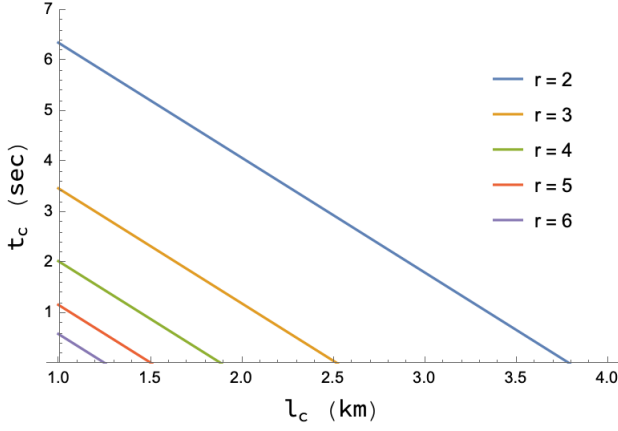


FIG. 5: In this figure, we consider a repeater-based network and plot the critical storage time t_c as a function of critical fiber length l_{cr} for the different numbers of repeater stations. We set $p_* = 0.5$, $\alpha = 1/22 \text{ km}^{-1}$, $\beta = 1/50 \text{ sec}^{-1}$, $q = 1$ and $\eta = 0.999$. (Color online)

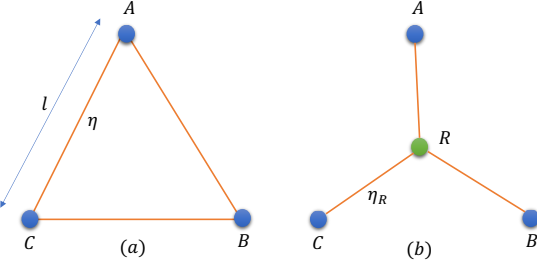


FIG. 6: In this figure we show (a) repeater-less triangle mesh network and (b) star-repeater network. For the same number of nodes, the repeater network in (b) reduces the channel loss for the mesh network topology in (a). (Color online)

η_e [168, 169].

Limitations on quantum network topologies

Let us consider an equilateral triangle-mesh network having the set of nodes $\mathbb{V} := \{v_A, v_B, v_C\}$ as shown in Fig. 6. The nodes of the triangle network are connected by qubit erasure channels having transmittance $\eta = e^{-(\alpha l + \beta t)}$, where l denotes the distance between the nodes and t is the time it takes for some resource χ to pass through the channel. Let us introduce a repeater scheme in the form of a star network as shown in Fig. 6 to effectively mitigate the losses due to transmission. The star network has virtual channels connecting the repeater node v_R to the node $v_i \in \mathbb{V}$. The transmittance of the virtual channels η_R is greater than η .

Assumption 1. *Let us assume there exist repeater-*

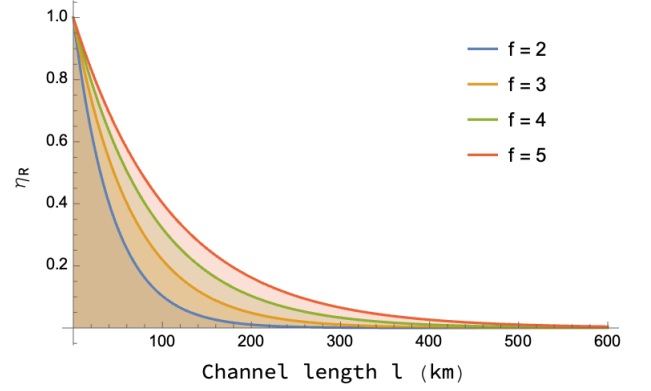


FIG. 7: In this figure, we plot the variation of η_R as a function of the channel length l (km) (setting $\beta = 0$) for different values of f . (Color online)

based quantum communication or quantum key distribution schemes that can mitigate the loss due to transmittance of a quantum channel such that the rate of communication (ebits or private bits per channel use [13]) is effectively of the order

$$\eta_R = \eta^{1/f} \quad (28)$$

in some regime (distance), where η is the transmittance of the channel and for some $f \geq 1$ (cf. [9, 171–173]).

In Eq. (28), the case of $f = 1$ has been shown in [13] for measurement-device-independent quantum key distribution (see [169, 170] for quantum key distribution over point-to-point channel) and the case of $f = 2$ has been shown in [9, 171–174] for twin-field quantum key distribution and asynchronous measurement-device-independent quantum key distribution [111, 175]. In Fig. 7, we set $\beta = 0$ and plot the variation of η_R as a function of the channel length l for different values of f .

Consider the task of sending ebits or private bits over the qubit erasure channel at a rate greater than p_* . To successfully perform the task, the critical length l_c and the critical time t_c are related via the expression

$$\alpha l_c + \beta t_c \leq -f \ln p_*. \quad (29)$$

We see from Eq. (29) that using repeaters provides f -fold advantage over repeater-less networks. We plot in Fig. 8 the critical length l_c and critical time t_c for sending ebits or private bits over the channel at a rate $p_* = 0.5$ for different values of f . In the plot, we have set $\alpha = 1/22 \text{ km}^{-1}$, and $\beta = 1/10 \text{ s}^{-1}$.

In the analysis of networks represented as graphs, it is important to analyze the robustness of the network for different information processing tasks. In recent works, the robustness has been studied in the context of removal of network nodes [176] and has been modelled as a percolation process on networks [69, 177, 178] represented as graphs. In these studies, the vertices are considered present if the nodes connecting them are functioning nor-

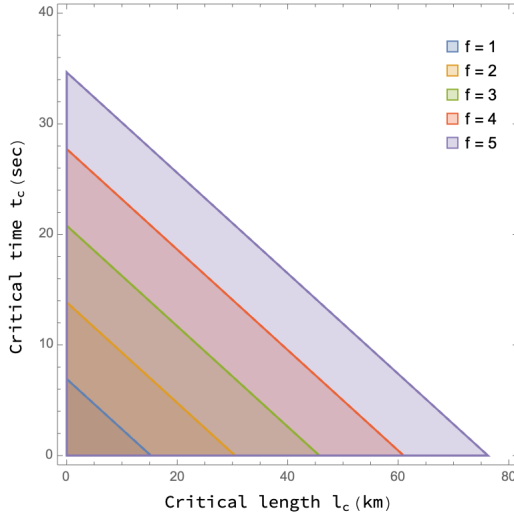


FIG. 8: In this figure, we plot the critical length l_c (km) and critical time t_c (sec) for sending ebits or private bits over the channel at a rate of $p_* = 0.5$ for different values of f . We have considered $\alpha = 1/22 \text{ km}^{-1}$ and $\beta = 1/10 \text{ sec}^{-1}$. (Color online)

mally. In the following subsection, taking motivations from degree centrality [179], betweenness centrality [180] and Gini index [181] of network graphs we present figures of merit to compare the robustness of network topologies. We then compare different network topologies based on these measures.

C. Robustness measure for networks

Networks that have a large number of edges are more tolerant to non-functioning nodes and edges as compared to those with fewer edges. Taking motivation from the degree centrality of a graph [179], we define the link sparsity of a network to assess the performance of a network.

Definition 7. Consider a network $\mathcal{N}(G(\mathbb{V}, \mathbb{E}))$ having the effective success matrix as \mathbb{U}_* . Let the total number of entries and the number of non-zero entries in \mathbb{U}_* be m and m_* respectively. The link sparsity of such a network is given by

$$\Upsilon(\mathcal{N}) = 1 - \frac{m_*}{m}. \quad (30)$$

The networks represented as graphs can exist in different topologies and have the same number of nodes, edges and also the same weighted edge connectivity. These networks are said to be isomorphic to one another.

Definition 8. (Graph isomorphism [134]) The graphs $G(\mathbb{V}, \mathbb{E}, \mathbb{L})$ and $G'(\mathbb{V}', \mathbb{E}', \mathbb{L}')$ are isomorphic iff there exists a bijective function $f: \mathbb{V} \rightarrow \mathbb{V}'$ such that:

$$1. \forall u \in \mathbb{V}, l \in \mathbb{L}, l' \in \mathbb{L}', l(u) = l'(f(u))$$

$$2. \forall u, v \in \mathbb{V}, (u, v) \in \mathbb{E} \leftrightarrow (f(u), f(v)) \in \mathbb{E}'$$

$$3. \forall (u, v) \in \mathbb{E}, l \in \mathbb{L}, l' \in \mathbb{L}', l(u, v) = l'(f(u), f(v))$$

It follows from Eq. (30) that isomorphic networks have the same value of link sparsity. Networks having the same value of link sparsity can differ in the distribution of edge weights. Taking motivation from the betweenness centrality of a graph [180], we define the connection strength of the nodes in the network and the total connection strength of the network.

Definition 9. Consider a network $\mathcal{N}(G(\mathbb{V}, \mathbb{E}))$ with $|\mathbb{V}| = N_v$ having the adjacency matrix and the effective success matrix as \mathbb{A}_* and \mathbb{U}_* . The connection strength of a node v_i in the network \mathcal{N} is given by

$$\zeta_i(\mathcal{N}) := \begin{cases} \left(\sum_{j \neq i} 2^{-[\mathbb{A}_*]_{ij}} \right) / N_v & \text{non-cooperative,} \\ \left(\sum_{j \neq i} [\mathbb{U}_*]_{ij} \right) / N_v & \text{cooperative.} \end{cases} \quad (31)$$

The total connection strength of the network \mathcal{N} in the (non-)cooperative strategy is obtained by adding the connection strengths of the individual nodes and is given by

$$\Gamma(\mathcal{N}) = \sum_j \zeta_j(\mathcal{N}). \quad (32)$$

Next, taking motivation from the Gini Index of network graphs [181] and using the definition of the connection strength of the nodes in a network, we define the sparsity index of the network.

Definition 10. Consider the plot with the fractiles of the order of nodes in the network $\mathcal{N}(G(\mathbb{V}, \mathbb{E}))$ along the horizontal axis and the cumulative sum of $\zeta_i(G)$ s along the vertical axis. The sparsity index of the network \mathcal{N} is given by

$$\Xi(\mathcal{N}) = \frac{\text{area enclosed by the curve and } x\text{-axis}}{\text{area enclosed by the } 45^\circ \text{ line}}. \quad (33)$$

As an example, the star network in Fig. 9 has a sparsity index of 1.22928 (see Appendix H for details). The sparsity index $\Xi(\mathcal{N})$ of the network \mathcal{N} measures the extent of inequality in the distribution of connection strength among the nodes of the network. High values of Ξ indicate a high cumulative percentage of connection strength for the cumulative fractile of the nodes. Typically it is desirable for the network to have low values of link sparsity and high values of sparsity index. In the following subsection, we compare the robustness measures for different network topologies.

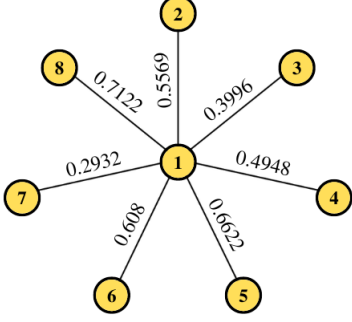


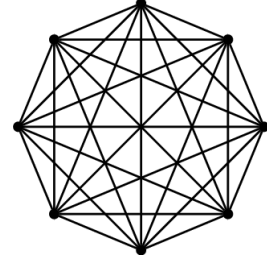
FIG. 9: In this figure, we present a star network with 8 nodes. The node v_1 is the hub and nodes v_2 to v_8 are the outer nodes. The functioning of the hub node is critical to the functioning of the network. (Color online)

D. Comparison of the robustness of network topologies

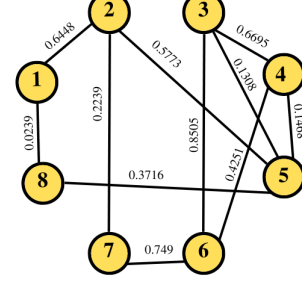
The topology of a network is defined as the arrangement of nodes and edges in the network. The information processing task that the network is performing decides the topology of the network. Two of the most commonly used network topologies are the star and mesh topologies.

A star network topology [182] of n nodes is a level 1 tree with 1 root node and $n-1$ leaf nodes. A star network with 8 nodes is shown in Fig. 9. The root node labelled 1 is the hub node and acts as a junction connecting the different leaf nodes labelled 2 to 8. Among all network topologies, this network typically requires the minimum number of hops for connecting two nodes that do not share an edge between them. The working of the hub is most critical to the functioning of the star network. The failure of a leaf node or an edge connecting a leaf node to the root does not affect the rest of the network. As an example of its use, this type of network finds application as a router or a switch connecting a ground station to different locations in an entanglement distribution protocol. In such a protocol, an adversary can attack the root node to prevent the proper functioning of the network. If the root node fails to operate, all leaf nodes connected to it become disconnected.

In a mesh topology [183], each node in the network shares an edge with one or more nodes, as can be seen from Fig. 10a and 10b. There are two types of mesh topologies depending on the number of edges connected to each node. A mesh is called fully connected if each node shares an edge with every other node of the network, as shown in Fig. 10a. A mesh is called partially connected if it is not fully connected, as shown in Fig. 10b. A mesh where each node shares an edge with only one other node of the network is called a linear network. In a partially or fully connected mesh, the presence of multiple paths between two nodes of the network makes it robust. As



(a) Fully connected mesh with 8 nodes



(b) A partially connected mesh with 8 nodes.

FIG. 10: In this figure, we present (a) fully connected and (b) partially connected mesh networks with 8 nodes. In a fully connected mesh network, there are edges between every pair of nodes. The presence of multiple paths between two nodes of the mesh network makes it more robust as compared to a star network with the same number of nodes. (Color online)

an example of its use, a mesh network can be used for a satellite-based entanglement distribution, which we discuss in detail in a later section.

Let us consider a mesh network $\mathcal{N}_m(G_m(\mathbb{V}, \mathbb{E}))$ of diameter d with $|\mathbb{V}| = N_v$ and for $(v_i, v_j) \in \mathbb{E}$, $p_{ij} = p$. Let there be a non-cooperating strategy for sharing resources between the nodes of the network. For such a strategy, the rows of the adjacency matrix of the network have N_z number of zero entries where $0 \leq N_z \leq N_v - 1$. Next, let there also exist a cooperating strategy for sharing resources between the nodes of this network. For such a strategy, the node v_i of the network does not share an edge with N'_z number of nodes where $0 \leq N'_z \leq N_z \leq N_v - 1$. From the remaining nodes, there exists edges between v_i and $(N_v - N'_z - 1)/d$ number of nodes with $p_{ij} = p^j$ where $1 \leq j \leq d$. For such a network, we have the link sparsity as

$$\Upsilon(\mathcal{N}_m) := \begin{cases} (N_z + 1)/N_v & \text{non-cooperating,} \\ (N'_z + 1)/N_v & \text{cooperating.} \end{cases} \quad (34)$$

The connection strength of the node v_i is given by

$$\zeta_i(\mathcal{N}_m) := \begin{cases} [1 + p(N_v - N_z)]/N_v & \text{non-cooperating,} \\ [1 + \frac{p(p^d - 1)(N_v - N'_z - 1)}{d(p - 1)}]/N_v & \text{cooperating.} \end{cases} \quad (35)$$

The total connection strength of the network is given by $\Gamma(\mathcal{N}_m) = N_v \times \zeta_i(\mathcal{N}_m)$. It can be seen that for this network the sparsity index $\Xi(\mathcal{N}_m)$ is the same as the connection strength of the node. This follows from the equal distribution of the weights in the network.

Next consider a star network $\mathcal{N}_s(G_s(\mathbb{V}, \mathbb{E}))$ with $|\mathbb{V}| = N_v$ and for $(v_i, v_j) \in \mathbb{E}$ we have

$$p_{ij} := \begin{cases} p & \text{if } i = 1 \text{ and } p \geq p_*, \\ 0 & \text{otherwise.} \end{cases} \quad (36)$$

The link sparsity of such a network is $\Upsilon(\mathcal{N}_s) = 1 - (1/N_v)$ for the cooperative strategy and $\Upsilon(\mathcal{N}_s) = 1 - [(3N_v - 2)/N_v^2]$ for the non-cooperative strategy. The connection strength of the root node is $\zeta_i(\mathcal{N}_s) = (1 + p(N_v - 1))/N_v$, while for the leaf nodes is

$$\zeta_i(\mathcal{N}_s) := \begin{cases} (1 + p)/N_v & \text{non-cooperative,} \\ [1 + p + p^2(N_v - 2)]/N_v & \text{cooperative.} \end{cases} \quad (37)$$

The sparsity index of the network is

$$\Xi(\mathcal{N}_s) := \begin{cases} [N_v^2 + p(N_v^2 + N_v - 2)]/N_v^3 & \text{non-cooperative,} \\ [N_v^2 + p(N_v - 1)(N_v + 2) + p^2(N_v - 2)(N_v - 1)]/(N_v + 1)/N_v^3 & \text{cooperative.} \end{cases} \quad (38)$$

As another example, consider a network $\mathcal{N}(G(\mathbb{V}, \mathbb{E}))$ having $|\mathbb{V}| = N_v$ number of nodes, and each node shares an edge with d other nodes. The effective adjacency matrix \mathbf{A}_* of such a network is a circulant matrix. Let the success probability of transferring a resource between the node 1 and the node n be given by,

$$p_{1n} := \begin{cases} p^n & \text{if } n \leq d/2 \text{ and } d = \text{even,} \\ p^{d-n+1} & \text{if } n > d/2 \text{ and } d = \text{even,} \\ p^n & \text{if } n \leq (d+1)/2 \text{ and } d = \text{odd,} \\ p^{d-n+1} & \text{if } n > (d+1)/2 \text{ and } d = \text{odd.} \end{cases} \quad (39)$$

The first row of the adjacency matrix is formed by calculating the weights $w_*(e_{1n}) = -\log p_{1n}$. The k^{th} row is formed by taking the cyclic permutation of the first row with an offset equal to k . In the non-cooperative strategy, the link sparsity of the network is then given by

$$\Upsilon(\mathcal{N}) = 1 - \left(\frac{d+1}{N_v} \right), \quad (40)$$

and the connection strength of the node v_i is given by

$$\zeta_i(\mathcal{N}) := \begin{cases} \frac{(1+p)(p^{(d+1)/2-1})}{N_v(p-1)} & \text{if } d \text{ is odd,} \\ \frac{1}{N_v} \left[1 + \frac{2p(p^{d/2-1})}{(p-1)} \right] & \text{if } d \text{ is even.} \end{cases} \quad (41)$$

In the following subsection, we introduce measures for identifying the critical nodes of a given network.

E. Critical nodes in a network

The critical nodes of a network are the nodes that are vital for the proper functioning of the network. Removing any of these nodes can lead to some of the other nodes in the network being disconnected. Given a network $\mathcal{N}(G)$, we proceed to define a measure for the criticality of the nodes in G . For this, at first, taking motivation from [184], we define the clustering coefficient for the nodes of a given network.

Definition 11. For a network $\mathcal{N}(G)$, let $G_i(\mathbb{V}_i, \mathbb{E}_i)$ be a sub-graph of G formed by the neighbours of node $v_i \in \mathbb{V}$. Let $n_i = |\mathbb{V}_i|$ be the number of nodes present in G_i and $e_i = |\mathbb{E}_i|$ be the number of edges present in G_i with $p_{ij} \geq p_*$. The clustering coefficient of the node v_i is defined as

$$C_i = \frac{2 e_i}{n_i(n_i - 1)}. \quad (42)$$

The average clustering coefficient of a network is calculated by taking the average of C_i for all the nodes of the network. We next proceed to define the average effective weight of a network using Eq. (15).

Definition 12. For a network $\mathcal{N}(G)$, the average effective weight of a network denoted by \tilde{w}_* is defined as the mean of the effective weight between all the node pairs in the network and is expressed as

$$\tilde{w}_*(G) = \frac{1}{n(n-1)} \sum_{\substack{v_i, v_j \in \mathbb{V} \\ i \neq j}} w_*(e_{i \rightarrow \dots \rightarrow j}), \quad (43)$$

where $w_*(e_{i \rightarrow \dots \rightarrow j})$ is the effective weight associated with the path connecting the nodes v_i and v_j .

When two nodes (v_i, v_j) are disconnected, the effective weight $w_*(e_{i \rightarrow \dots \rightarrow j})$ becomes infinite. Small values of $\tilde{w}_*(G)$ indicate that the network performs the task with high efficiency.

Definition 13. For a network $\mathcal{N}(G)$, let us denote the shortest path connecting the node pairs $(v_i, v_j) \in G$ as $d_{ij} \in \mathbb{D}$. We define the centrality τ_i of the node v_i as the number of paths belonging to the set \mathbb{D} in which the node v_i appears as a virtual node. The critical parameter associated with the node v_i is defined as

$$\nu = \frac{\tau_i}{C_i \tilde{w}_*(G_i)}. \quad (44)$$

The critical nodes of a graph have high values of ν . These nodes of the network are essential for the proper functioning of the network. If one of these nodes is removed, it will lead to a decrease in the overall efficiency

of the network. Quantum network architectures have potential applications in diverse fields ranging from communication to computing. In the following section, we present the bottlenecks of some potential use of quantum networks for real-world applications.

V. REAL WORLD INSTANCES

In this section, we first present practical bottlenecks in the distribution of entangled states between two far-off cities. We then consider different currently available as well as near-future quantum processor architectures as networks and observe their robustness parameters. Then we propose networks for (a) the major international airports to communicate via a global quantum network and (b) the Department of Energy (DoE) at Washington D.C. to communicate with the major labs involved in the National Quantum Initiative (NQI) by sharing entanglement. We present the practical bottlenecks for such models.

A. Entanglement distribution between cities

Consider a satellite-based network for sharing an entangled state between two far-off cities. Let such a network be a two-layered model consisting of a global scale and a local scale. On a global scale, there are multiple ground stations located across different cities. Such ground stations are interconnected via a satellite network. Two ground stations share an entangled state using the network via the shortest network path between them (see Sec. VIA for details of the shortest path algorithm.) As an example, we show in Fig. 11 the shortest path connecting the ground stations located at Gauribidanur and Gdańsk via the global satellite network. On the local scale, the cities (end nodes) are connected to their nearest ground station via optical fibers. We show in Fig. 12 the local scale network for the ground station located at Gauribidanur and Gdańsk. The ground station at Gauribidanur is connected to the localities of Chikkabalapur, Bangalore, Hosur and Mysore. The ground station at Gdańsk is connected to the localities of Poznań and Warsaw.

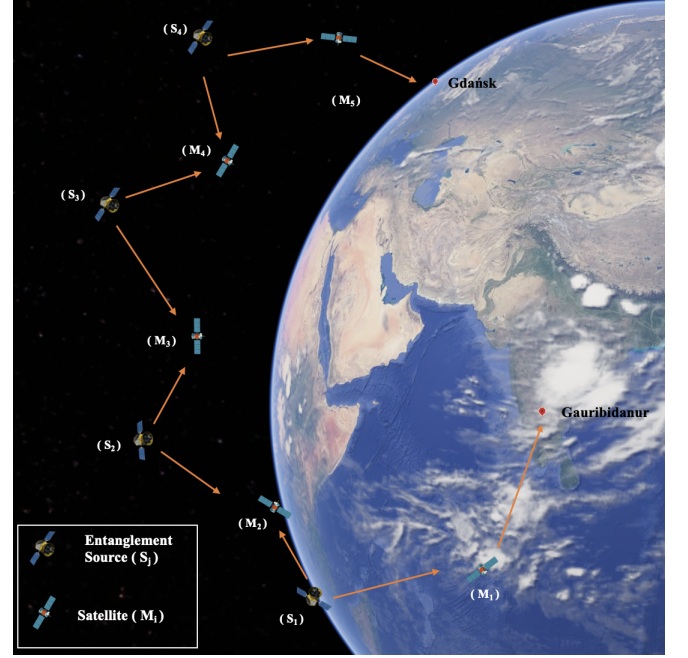


FIG. 11: In this figure, we present the shortest network path between the ground stations at Gauribidanur and Gdańsk via the global satellite network. The entangled sources are marked as S_i and the satellite stations are marked as M_i . The shortest path has 6 entangled sources and 5 satellite stations. The image was created using the Google Earth software [185]. (Color online)

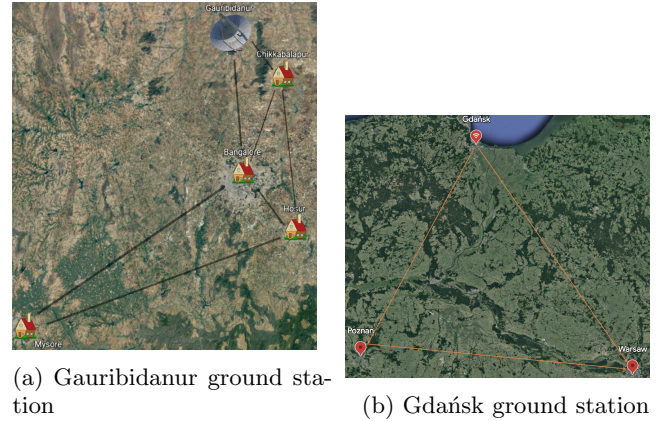


FIG. 12: In this figure, we present the local scale network architectures at (a) Gauribidanur and (b) Gdańsk for sharing entanglement across nearby localities. The ground stations are connected to multiple localities via optical fibers (shown in black and orange lines). The images were created using Google Earth software [185]. (Color online)

In the satellite network, there are sources (S_j) producing entangled photonic qubit pairs in the state Ψ^+ . The source then sends the photons belonging to a pair to different neighbouring satellites via a quantum channel

as shown in Fig. 11. We model the quantum channel between the ground station and the satellite at the limits of the atmosphere as a qubit thermal channel (see Sec. D3 and Sec. E) and that between two satellites as an erasure channel (see Sec. D2) having erasure parameter η_e . The erasure channel parameter is assumed to be identical throughout the network. The satellite stations M_j outside the limits of the atmosphere perform Bell measurement on their share of the qubits that they received from their neighbouring source stations. The satellites on the boundary of the atmosphere transmit their share of qubit via the atmospheric channel to the ground stations (which we call local servers). The ground stations on receiving the state store it in a quantum memory. In the quantum memory, the state evolves via a depolarising channel (see Sec. D1). The local servers distribute the quantum states to different localities (which we call clients) on request using optical fibers as can be seen in Fig. 12.

Let the shortest network path between the ground stations at Gauribidanur and Gdańsk have 5 satellites and 4 entangled photon sources as shown in Fig. 11. The entanglement yield of the network is given by

$$\xi_{\text{avg}} = \eta_t^G (\eta_e^2)^4, \quad (45)$$

where η_t^G is obtained from Eq. (D18) and takes into account the local weather conditions at Gauribidanur and Gdańsk. In the general network with n satellite-to-satellite links between the two ground stations, the average entanglement yield is given by

$$\xi_{\text{avg}} = \eta_t^G (\eta_e^2)^n. \quad (46)$$

With the motivation to perform delegated quantum computing [28–30, 155, 186] by accessing the IBM Quantum Hub at Poznań [143], let the Indian Space Research Organisation (ISRO) headquarter¹ at Bangalore connected to the Gauribidanur ground station request to securely communicate with Poznań by sharing an entangled state. To enable routing of the quantum states at the ground stations, we introduce the following queuing discipline (see Sec. VID).

The ground stations store the incoming qubits in different quantum memory slots and serve the receiving traffic² requests from different local clients. The total number of memory slots available in the quantum memory is fixed. The evolution of the stored qubits in the quantum memory is modelled via a depolarising channel with channel parameter p . We model the quantum memory as a max-

heap data structure (see Definition 3) with the key as the fidelity of the stored quantum state. If the fidelity of any quantum state stored in the memory drops below a pre-defined critical value, η_{crit} , that state is deleted from the memory. We note that the value of η_{crit} is determined by the task or the protocol that the end parties may be interested in performing using their shared entangled state. On receiving a connection request from a single local client, the ground station transmits the latest qubit that it has received as outward traffic. Now when the ground station receives traffic requests from multiple local clients, there is the problem of optimizing the traffic flow³. For such a flow problem, we introduce the following modified fair queuing algorithm.

Let us define $t_p^{(i)}$ as the time to process the i^{th} quantum state in the memory, $t_i^{(i)}$ as the starting time for the transmission from the memory and $t_f^{(i)}$ as the time when the state has been transmitted from the memory. We then have,

$$t_f^{(i)} = t_i^{(i)} + t_p^{(i)}. \quad (47)$$

Now, there is a possibility that the state has arrived at the memory before or after the processing of $i - 1$ states in this heap. In the latter case, the state arrives at an empty heap memory and is transmitted immediately if there is a traffic request. In the other case, it swims through the heap depending on its fidelity and is stored in the memory. Let us denote $t_r^{(i)}$ as the time required for the node to swim up to the root node from its current position in the heap. Then we have,

$$t_f^{(i)} = \max \left(t_f^{(i-1)}, t_r^{(i)} \right) + t_p^{(i)}, \quad (48)$$

where $t_f^{(i-1)}$ is the time required for processing $(i - 1)^{\text{th}}$ quantum state. If there are multiple flows, the clock advances by one tick when all the active flows receive one state following the qubit-by-qubit round-robin basis. If the quantum state has spent s time steps in the memory then the average entanglement yield is given by

$$\xi_{\text{avg}} := \begin{cases} \eta_d^s \eta_t^G (\eta_e^2)^n & \text{if } \eta_d^s > \eta_{\text{crit}}, \\ 0 & \text{otherwise,} \end{cases} \quad (49)$$

where η_d is obtained from Eq. (D6) and takes into account the loss in yield per time step in the quantum memory. Let us assume the ground station at Gauribidanur and Gdańsk transmits the state via identical fibers to ISRO at Bangalore and Poznań, respectively. Considering the fiber losses at the two ground stations given by $e^{-\alpha l_B}$ and $e^{-\alpha l_M}$, the sources producing the state Ψ^+ with probability η_s , and assuming that the quantum state

¹ As we were finalizing the paper, we learnt that ISRO was successful in soft landing of its spacecraft **Chandrayaan-3** (Vikram lander and Pragyan rover) on the Moon's south polar region on 23-08-2023 at 18:03 IST.

² Traffic is the flow of photons between the nodes of the network for enabling the network to perform a specific information processing task.

³ Traffic flow is a sequence of quantum states that is sent from the ground station to the local station.

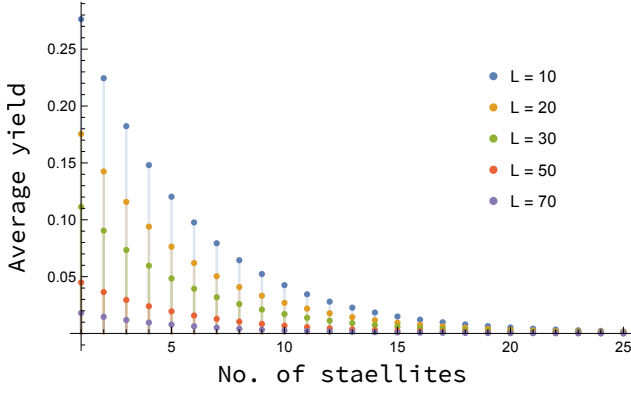


FIG. 13: In this figure, we plot the average yield ξ_{avg} (see Eq. (51)) as a function of the number of satellites in the network for different values of the total optical fiber length $L = l_B + l_M$ (shown figure inset). We set $\eta_s = 0.9, s = 1, p = 0.1, \eta_e = 0.95, \eta_1 = 0.5, n_1 = 0.5, \alpha = 1/22 \text{ km}^{-1}$. (Color online)

has spent s time steps in the memory, the average entanglement yield is given by

$$\xi_{\text{avg}} = \eta_d^s \eta_t^G (\eta_e^2)^n (\eta_s)^{n-1} e^{-\alpha(l_B + l_M)}, \quad (50)$$

where l_B and l_M are the lengths of the fibers from ISRO Bangalore and Poznań to the Gauribidanur and Gdańsk ground stations respectively. Inserting η_t^G from Eq. (D18), we have the yield given by

$$\begin{aligned} \xi_{\text{avg}} &= e^{-\alpha(l_B + l_M)} (\eta_e^2)^n \eta_s^{n-1} \\ &\left[(1-p)^{2s} - \frac{1}{4}(p-2)p \left((s-1)(1-p)^{2(s-1)} + 1 \right) \right] \\ &\left[(n_1 - 1)n_1(\eta_1 - 1)^2 + \frac{1}{2}(1 + \eta_1^2) \right] \end{aligned} \quad (51)$$

where η_1, n_1 take into account the local weather condition at Gauribidanur and Gdańsk and s is the number of applications of depolarising channel per unit time in the quantum memory. We plot in Fig. 13, the average entanglement yield ξ_{avg} of two cities connected by the network as a function of the number of satellite-to-satellite links n between their nearest ground stations for different values of the total optical fiber length $L = (l_B + l_M)$. We observe that for a fixed value of L , ξ_{avg} decreases with an increase in n . Also, for a fixed value of n , ξ_{avg} decreases with increase in L . Furthermore, we plot in Fig. 14 and 27 the variation in ξ_{avg} as a function of n for different single photon source architectures having efficiencies η_s . We observe that for a given source efficiency η_s , ξ_{avg} decreases with increase in n . Also, we observe that Quantum dot-based, atom-based, and SPDC-based entangled photon sources are best suited for the entanglement distribution network.

Our methods in general apply to sharing multipartite entangled states among different ground stations dis-

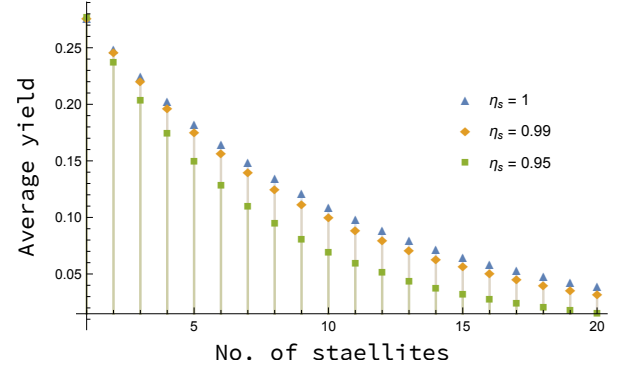


FIG. 14: In this figure, we plot the average yield ξ_{avg} (see Eq. (51)) as a function of the number of satellites in the network for single photon source architectures. The single photon source architectures have the source efficiencies (a) $\eta_s = 0.95$ (b) $\eta_s = 0.99$ and (c) $\eta_s = 1$.

For this, we set $L = l_B + l_M = 10 \text{ km}, s = 1, p = 0.95, \eta_e = 0.95, \eta_1 = 0.5, n_1 = 0.5, \alpha = 1/22 \text{ km}^{-1}$. (Color online)

tributed at different geographical locations across the globe. To observe this, note that if certain users of the network share bipartite entangled states, then such states can be used to distill multipartite entangled states with the use of ancilla and entanglement swapping protocols [13, 187, 188].

B. Quantum Processors

The currently available quantum processors (QPUs) use different technologies to implement the physical processor. The processors of IonQ and Honeywell utilize a trapped ion-based architecture, while IBM, Rigetti, and Google have a superconducting architecture. The superconducting architecture requires physical links between qubits that are to be entangled, while the trapped ion-based architecture does not have any topological constraint. In this section, we model the different quantum processor architectures as graphical networks (see Table I) and present the robustness measures (defined in Sec. IV C) for such networks.

We consider different qubit quantum processor network architectures in square, heavy-hexagonal and octagonal layouts. The link sparsities of each unit cell⁴ for these different network layouts are given by

$$\Upsilon(N) := \begin{cases} 1 - \left(\frac{16}{64}\right) \approx 0.75 & \text{octagonal,} \\ 1 - \left(\frac{8}{16}\right) \approx 0.5 & \text{square,} \\ 1 - \left(\frac{24}{144}\right) \approx 0.833 & \text{heavy hexagonal.} \end{cases} \quad (52)$$

⁴ Unit cell is the smallest group of processor qubits which has the overall symmetry of the processor, and from which the entire processor can be constructed by repetition.

Name	Layout	Fidelity	Qubits	T_1
Sycamore (Google) [139]	square lattice	96.9% (RO) 99.85% (1Q) 99.64% (2Q)	54	15 μs
Eagle (IBM) [140, 141]	heavy hexagonal	99.96% (RO) 99.99% (1Q) 99.94% (2Q)	127	95.57 μs
Aspen-M-2 (Rigetti) [142]	octagonal	97.7% (RO) 99.8% (1Q) 90% (2Q)	80	30.9 μs

TABLE I: The performance details of different quantum processors. In the above table, the second column provides the arrangement of the qubits in the processor. The third column provides the 1 qubit (1Q), 2 qubits (2Q), and the readout (RO) fidelity of the processors. The fourth column provides the total number of qubits in the processor, and the fifth column provides the thermal relaxation time (T_1) of the qubits of the processor.

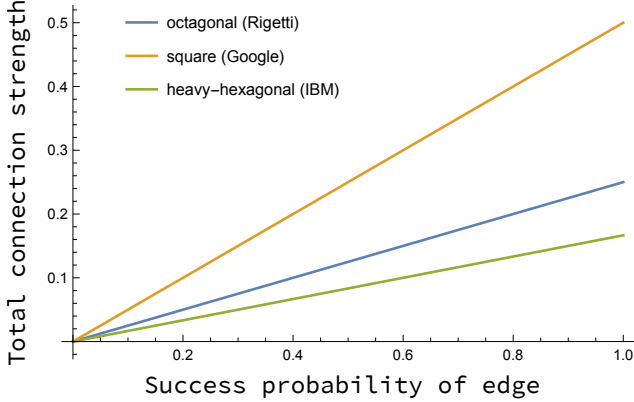


FIG. 15: In this figure, we assume that all the edges have the same weight, and we plot the total connection strength as a function of the edge weight. For this, we consider three processor designs by (a) Rigetti [142] (octagonal lattice), (b) Google [139] (square lattice), and (c) IBM [140, 141] (heavy-hexagonal lattice). (Color online)

We observe that the square structure has the lowest link sparsity, followed by octagonal and heavy hexagonal structures. Next, let the edges present in these network layouts have success probability p . The connection strength of the i^{th} node in the unit cell of octagonal, heavy hexagonal and square network for a non-cooperative strategy is given by

$$\Gamma(N) := \begin{cases} p/4 & \text{octagonal,} \\ p/2 & \text{square,} \\ p/6 & \text{heavy hexagonal.} \end{cases} \quad (53)$$

We plot in Fig. 15 the connection strength of the i^{th} node

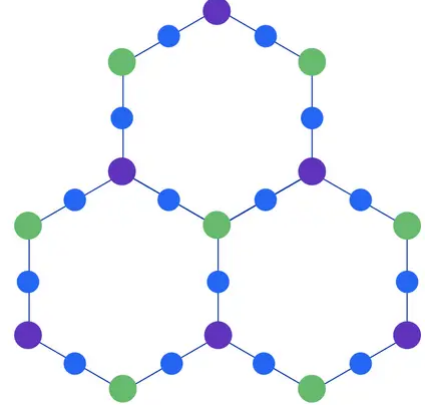


FIG. 16: A slice of a quantum processor model based on heavy-hexagonal structure discussed in [189]. The link sparsity of the unit cells in the network is 0.833, and the critical nodes of the network slice are shown in green and violet. (Color online)

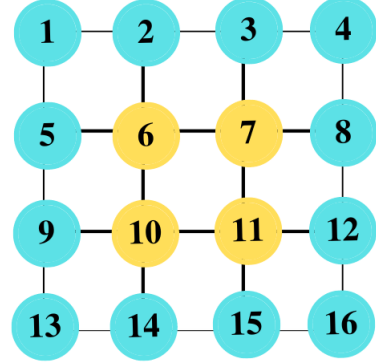


FIG. 17: A 4×4 slice of a 1024 node quantum processor architecture based on square structure. The total network layout is represented as a 32×32 lattice. The link sparsity of the network is 0.9962, and the critical nodes of the network slice are shown in yellow. (Color online)

for different values of the success probability of edge. We observe that the connection strength for a given success probability of edge is highest for square networks, followed by octagonal and heavy-hexagonal networks.

We propose a 1024-node square lattice-based quantum processor network architecture represented as a 32×32 lattice. We show in Fig. 17 a 4×4 slice of the lattice as a representation of the entire quantum processor. The link sparsity of the 1024 node square network is 0.9962. The nodes shown in yellow in Fig. 17 are identified as critical nodes. We observe in Fig. 17 that there are three types of nodes in the network based on the number of edges that are connected to the node. We call a node a corner node, edge node, and inner node if it shares an edge with two, three, and four other nodes, respectively. The connection strength of these three types of nodes is

given by

$$\zeta_i(\mathcal{N}) := \begin{cases} p/256 & \text{inner node,} \\ 3p/1024 & \text{boundary node,} \\ p/512 & \text{corner node.} \end{cases} \quad (54)$$

C. Network propositions

Let us first consider a network connecting all the major airports in the world. We say that two airports are connected if there exists at least one commercial airline currently operating between them. We consider a network consisting of 3463 airports all over the globe forming the nodes of the network and 25482 edges or airline routes between these airports [190]. For such a network, we note that the longest route is between Singapore, Changi International Airport, and New York John F. Kennedy International Airport, in the United States, with a distance of approximately 15331 km. The average distance between the airports in the network is approximately 1952 km. We propose a quantum network with airports as nodes and the connections between the airports as edges. We define the edge weight of the edge connecting the nodes $\{v_i, v_j\}$ of the network as

$$w(e_{ij}) := \begin{cases} e^{-L_{ij}/22} & \text{if } L_{ij} < 50 \text{ km} \\ 0.8 & \text{if } L_{ij} \geq 50 \text{ km} \end{cases} \quad (55)$$

where L_{ij} is the distance between two airports denoted by nodes v_i and v_j . The link sparsity of such a network is 0.99575, and the total connection strength is given by 0.99787. We observe that the most critical airports present in this network are Istanbul International Airport, Dubai International Airport, Anchorage Ted Stevens in Alaska, Beijing Capital International Airport, Chicago O'Hare International Airport, and Los Angeles International Airport.

Let the airports of the network require to securely communicate with each other. The sharing of entangled states among the airports is a primitive for secure communication among them. Let us assume all these airports are located at the same altitude. Let the ground stations located at the airports share an entangled state using a global satellite-based mesh quantum network as described in Sec. V A. The ground stations connect to the satellite network via the atmospheric channel modelled as a qubit thermal channel. The satellites of the network are interconnected via a qubit erasure channel. For two airports a_1 and a_2 requiring to connect, the average entanglement yield is given by

$$\begin{aligned} \xi_{\text{avg}} &= \eta_t^a (\eta_e^2)^n \\ &= (\eta_e^2)^{\lfloor \frac{L}{L_0} \rfloor} \left[(n_1 - 1)n_1(\eta_1 - 1)^2 + \frac{1}{2}(1 + \eta_1^2) \right], \end{aligned} \quad (56)$$

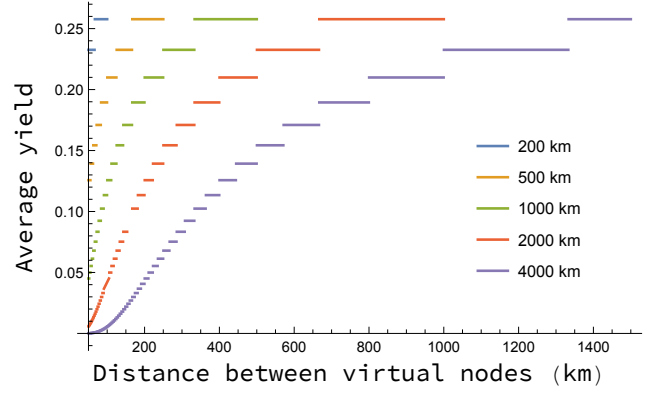


FIG. 18: In this figure, we plot the average yield ξ_{avg} (see Eq. (56)) as a function of the distance between the virtual nodes for different lengths between the airports.

For this, we set $\eta_e = 0.95, \eta_1 = 0.5, n_{21} = 0.5$. (Color online)

where L denotes the distance between a_1 and a_2 . L_0 denotes the distance between the nodes of the satellite network. We assume identical atmospheric conditions at a_1 and a_2 and set $\eta_e = 0.95, \eta_1 = 0.5$ and $n_1 = 0.5$. With these choices of parameters, we present in Fig. 18 the average yield as a function of the distance between the nodes of the satellite network for different values of L . The entanglement yield between the airports for different channel parameters not considered in this section can be obtained from Eq. (56).

The quantum Internet can be used for secure communication between a central agency and end parties. It may be desirable here for the central agency to prevent direct communication between the end parties. As an example, consider the U.S. Department of Energy (DoE) in Washington D.C. require to securely communicate by sharing entangled states with the major labs [191] that are involved in The National Quantum Initiative (NQI) using the Star network. The DoE is at the hub node of such a network and the different labs are the leaf nodes. For each edge of the network, let there be independent fiber-based repeater chain networks (described in Sec. III.) Let each edge present in the network have a success probability $p = e^{-\alpha L/n}$ where α is the channel loss parameter, L is the total distance between the DoE and the lab, and n is the number of virtual nodes. Using Eq. (G4), we obtain the upper bound on α as

$$\alpha < \frac{\log(3)}{L(1 + \frac{1}{n})}. \quad (57)$$

For different labs, we plot in Fig. 19 the upper bound on α for different values of n . In the figure, we have considered some of the major labs, which can be extended to all other labs involved in the NQI. In the following section, we present graph algorithms that are primitives for implementing different information-processing tasks using the quantum Internet.

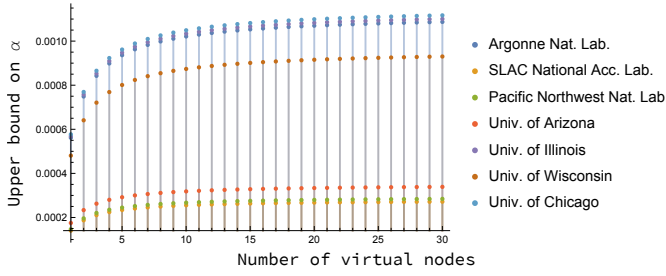


FIG. 19: The upper bound on the channel parameter α for sharing entanglement between the U.S. Department of Energy (DoE) at Washington D.C. and some other labs [191] involved in The National Quantum Initiative (NQI). In this network, the DoE is the hub node while the labs are at the outer nodes. The edge connecting the hub to an outer node represents a repeater relay network. (Color online)

VI. ALGORITHMS

In Sec. VI A, we provide an algorithm to find the shortest path between a pair of end nodes. We then provide an algorithm in Sec. VI B to constrict a network architecture for sharing resources between two parties, each having multiple nodes. In Sec. VI C, we provide an algorithm to identify the critical nodes of a given network. Then in Sec. VI D, we provide an algorithm to optimize the flow of resources at a node having multiple input and output channels.

A. Shortest path between a pair of nodes

Let us consider a network \mathcal{N} represented as a graph G . We consider the task of finding the path between two given nodes in G that have the lowest effective weight for routing resources between them [192]. We call a path connecting two nodes in the network and having the lowest effective weight as the shortest path between them. Finding the shortest path between two nodes of a network is important as longer paths are more vulnerable to node and edge failures. To find the shortest path between two nodes, we introduce a modified version of Dijkstra's algorithm [193] in Algorithm 1. In Algorithm 1, the shortest spanning tree is generated with the source node as the root node. Then the nodes in the tree are stored in one set and the other set stores the nodes that are not yet included in the tree. In every step of the algorithm, a node is obtained that is not included in the second set defined above and has a minimum distance from the source.

Algorithm 1 Modified Dijkstra's algorithm

```

1: function DIJKSTRA( $G, S, \text{target}$ )
2:   Initialize:
    $pq \leftarrow$  empty min priority queue
    $\text{dist} \leftarrow \emptyset$ 
    $\text{pred} \leftarrow \emptyset$ 
3:   for every node in  $G$  do
4:     if node =  $S$  then
5:        $pq[\text{node}] \leftarrow 0$ 
6:     else
7:        $pq[\text{node}] \leftarrow \text{infinite}$ 
8:   for every node and minDist in  $pq$  do
9:      $\text{dist}[\text{node}] \leftarrow \text{minDist}$ 
10:    if node = target then
11:      break
12:    for every neigh of node do
13:      if neigh  $\in pq$  then
14:        score  $\leftarrow \text{dist}[\text{node}] +$ 
           $G[\text{node}, \text{neigh}][\text{weight}]$ 
15:        if score <  $pq[\text{neigh}]$  then
16:           $pq[\text{neigh}] \leftarrow \text{score}$ 
17:           $\text{pred}[\text{neigh}] \leftarrow \text{node}$ 
18:   return dist, pred

```

To obtain the shortest path between any two nodes of a given graph, we apply Algorithm 2 to implement the modified Dijkstra's algorithm. The algorithm returns the shortest path between the source node and the end node in the graph.

Algorithm 2 Obtaining the shortest path between the source and target nodes in a graph

```

1: Initialize:
   source  $\leftarrow$  starting node
   target  $\leftarrow$  target node
2:  $G \leftarrow$  the given graph
3:  $[\text{dist}, \text{pred}] \leftarrow \text{DIJKSTRA}(G, \text{source}, \text{target})$ 
4: end  $\leftarrow$  target
5: path  $\leftarrow$  [end]
6: while end  $\neq$  source do
7:   end =  $\text{pred}[\text{end}]$ 
8:   path.append(end)
9: disp(path)

```

Example 1. Let us consider a weighted graph with 8 nodes as shown in Fig. 20. A physical interpretation can be to consider the transfer of quantum states from node v_i to node v_j via quantum channels denoted by the edges. The edge weight between the nodes v_i and v_j is given by $-\log p_{ij}$ where p_{ij} is the success probability of sharing the resource between these two nodes. The shortest path connecting the nodes would then provide the highest success probability for the task. If we consider the source as node v_8 and the target as node v_6 , then the algorithm returns the shortest path as $v_8 \leftrightarrow v_1 \leftrightarrow v_3 \leftrightarrow v_6$. It may be desirable for another node say v_7 to share a re-

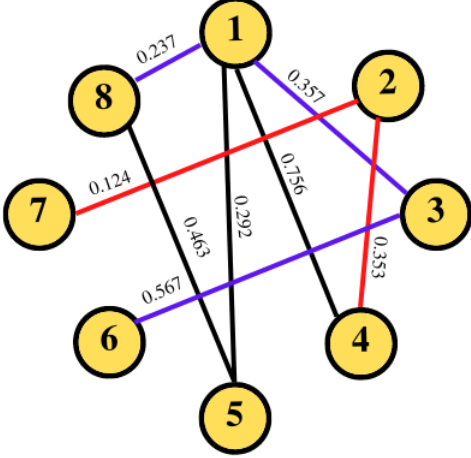


FIG. 20: A network represented by a weighted graph with 8 nodes. Multiple pairs of nodes can share resources using this network. As an example, nodes (8, 6) can share resource via the path $8 \leftrightarrow 1 \leftrightarrow 3 \leftrightarrow 6$ (shown in blue), then nodes (7, 4) can share resource via the path $7 \leftrightarrow 2 \leftrightarrow 4$ (shown in red.) (Color online)

source with node v_4 using the same network. The node v_7 and v_4 can share resources via the path $v_7 \leftrightarrow v_2 \leftrightarrow v_4$ without involving the virtual nodes in the shortest path between (v_8, v_6) . We observe that multiple pairs of nodes can share resources using this network.

In the following subsection, we present an algorithm to construct a network for sharing resources between two parties each having multiple nodes.

B. Network Construction

Let two parties Alice (denoted by A) and Bob (denoted by B) require to share a resource using a mesh network. We assume that A and B have n_A and n_B number of nodes respectively. We introduce Algorithm 3 to obtain the structure of the mesh that ensures there exist distinct paths between nodes of A and B . In Algorithm 3, we impose the constraints that (a) at a time all nodes of A shall be connected to distinct nodes of B via the shortest available path with unique virtual nodes and (b) there exists a path between every nodes of A and B .

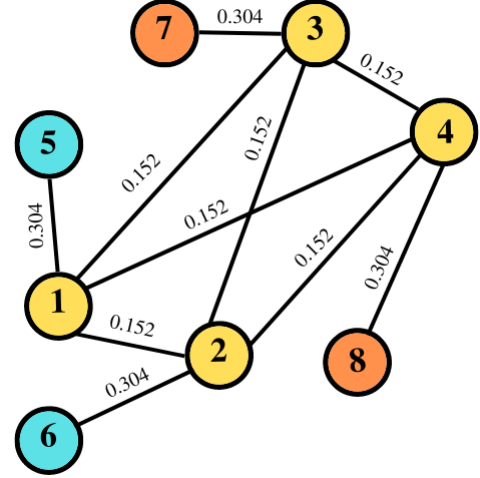


FIG. 21: A 4 node network (shown in yellow) constructed using Algorithm 3 for connecting the hubs A and B . The hubs A and B each have two nodes and are shown in orange and blue respectively. (Color online)

Algorithm 3 Network construction algorithm

```

1: function NETWORK( $n_A, n_B$ )
2:   Initialize:
     count  $\leftarrow n_A + n_B$ 
     g  $\leftarrow$  complete graph (no. of nodes: count)
     g[weight]  $\leftarrow$  mesh edge weights
3:   for every node  $i$  of  $A$  do
4:     add edge to g ( $i$ , count, weight)
5:     count  $\leftarrow$  count + 1
6:   for every node  $i$  of  $B$  do
7:     add edge to g ( $i$ , count, weight)
8:     count  $\leftarrow$  count + 1
   return g

```

Example 2. Consider two geographically separated companies A and B requiring to connect to each other via a mesh network. We call the headquarters of the companies as hubs. In Fig. 21 we show the hubs of A and B in blue and orange respectively. Using Algorithm 3 we obtain the network topology for which there exists distinct paths for possible pairs of (a_i, b_j) where $a_i \in A$ and $b_j \in B$.

In the following subsection, we consider a given network represented as a graph and present an algorithm to identify the critical nodes of the network.

C. Identifying the critical nodes

The critical nodes of the network are essential for the proper functioning of the network. If one of these nodes is removed, it will lead to a decrease in the overall performance efficiency of the network. We present Algorithm 4 to obtain the critical parameter ν for the nodes of the

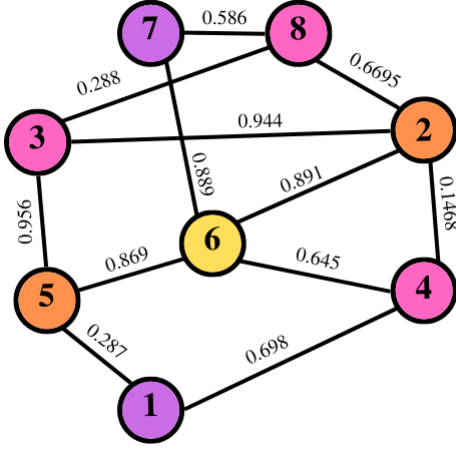


FIG. 22: A network represented by a weighted graph with 8 nodes and 12 edges. Node v_6 (shown in yellow) is the most critical node followed by nodes v_2 and v_5 (shown in orange). These nodes are the most critical for the proper functioning of the network. (Color online)

network using Eq. (44). The nodes with the highest values of ν are identified as the critical nodes of the network. These are the nodes that are the most important for the proper functioning of the graphical network.

Algorithm 4 Finding the critical nodes in a given graph

- 1: $G \leftarrow$ the given graph
 - 2: **for** every node in G **do**
 - 3: $C_i \leftarrow$ clustering coeff using Eq. (42)
 - 4: $\bar{w}_*(G) \leftarrow$ avg cost using Eq. (43)
 - 5: $\tau_i \leftarrow$ centrality of the node
 - 6: $\nu_i \leftarrow \tau_i / C_i \bar{w}_*(G)$
 - 7: $\text{critNodes} \leftarrow$ list of nodes with high values of ν_i .
-

Example 3. Let us use Algorithm 4 to obtain the critical nodes of the graph with 8 nodes shown in Fig. 22. We have the critical parameter for different nodes in the network as

node number (i)	ν_i	node number (i)	ν_i
v_1	0.1714	v_5	1.5238
v_2	1.6667	v_6	2.5714
v_3	0.7619	v_7	0.1714
v_4	0.9523	v_8	0.5714

We observe that node v_6 is the most critical followed by node v_2 and node v_5 . We label these nodes as the critical nodes of the network.

In the following subsection, we introduce an algorithm

for optimizing the flow of resources at a node that has multiple input and output channels.

D. Resource allocation at a node

The nodes of a network can have a buffer memory where resources such as incoming packets⁵ from different input channels can be stored and later distributed via different output channels to neighbouring nodes based on traffic request. We introduce Algorithm 5 for the optimal flow of resources at a node having multiple input and output channels.

Algorithm 5 Resource allocation at a node

Initialize:

$\text{buffSize} \leftarrow$ size of buffer

$\text{buffer} \leftarrow \emptyset$

procedure PRODUCER(thread)

while items produced and empty buffer slot **do**

 gain access to buffer

 store item at empty buffer slot

 update other memory slots as per task

 release the buffer

procedure CONSUMER(thread)

while buffer is not empty **do**

 gain access to buffer

 acquire item from the buffer

 update other memory slots as per task

 release the buffer

create and start all producer threads

create and start all consumer threads

In Algorithm 5, the procedures CONSUMER threads⁶ are the instances of the output channels that extract packets from the buffer and the PRODUCER are the instances for the input channels that inputs packets to the buffer.

VII. DISCUSSION

We envision that the implementation of the quantum Internet will follow a task-oriented approach. The underlying network structure at any stage of implementation is expected to provide loose coupling, meaning end users can perform information processing tasks without requiring to know the details of implementation, thereby reducing dependencies between different tasks. This requires assessing the practical limitations for implementing different tasks.

⁵ Packets are units of information or photons or resources that are transmitted across a network.

⁶ Thread is a sequential execution of tasks in a process.

Our work provides a step in that direction by taking a graph theory (and information theory-)based approach to analyze the scalability and robustness of the quantum Internet. Focusing on the latter part, we have provided measures for comparing the robustness and identifying the critical nodes of different network topologies. Identifying quantum processors as real-world mesh networks, we compared the robustness measures for the quantum processor architectures by Google, IBM and Rigetti. With the vision of having a 1024-qubit quantum processor in the future, we extend the 54-qubit layout by Google to include 1024 qubits and observe the robustness of such a network.

The network structure of the quantum Internet is determined by the information processing tasks that are implemented using it. Looking at the elementary link level, we have obtained bounds on the critical success probability for performing different tasks. Extending to a more general repeater-based network, we have obtained a trade-off between the channel length and the time interval for which the states can be stored at the nodes such that the shared state is useful for different tasks.

Looking at the specific details of implementation, considering repeater-based networks, we have provided the range of isotropic state visibility and an upper bound on the number of repeater nodes for distilling secret keys at non-zero rates via DI-QKD protocols. We have considered practical parameters like atmospheric conditions and imperfect devices in obtaining bottlenecks for implementing a satellite-based model distributing resources between far-off places. For such a network we have presented algorithms for implementing certain underlying network-related tasks such as obtaining the network layout, obtaining the network routing path and allocating resources at the network nodes. Overall, the assessment presented in this paper can be used in benchmarking the critical parameters involved in realizing the quantum Internet.

ACKNOWLEDGMENTS

AS thanks Keval Jain for the useful discussions. AS acknowledges the Ph.D. fellowship from the Raman Research Institute, Bangalore. MAS acknowledges support from the Summer Research InternSHIP on Technological Innovations (SRISHTI) held during the summer of 2022 at IIIT Hyderabad. KH acknowledges partial support from the Foundation for Polish Science (IRAP project, ICTQT, contract no. MAB/2018/5, co-financed by EU within Smart Growth Operational Programme). The ‘International Centre for Theory of Quantum Technologies’ project (contract no. MAB/2018/5) is carried out within the International Research Agendas Programme of the Foundation for Polish Science co-financed by the European Union from the funds of the Smart Growth Operational Programme, axis IV: Increasing the research potential (Measure 4.3). SD acknowledges support from

the Faculty Seed Grant by the IIIT Hyderabad.

Appendix A: Dual rail encoding of photons

In the dual rail encoding scheme [17], the qubits are encoded using the optical modes⁷ of photons. The computational basis of the photonic qubit system A encoded in the polarization modes m_1 and m_2 is given by

$$|H\rangle_A \rightarrow |1, 0\rangle_{l_1, l_2}, \quad |V\rangle_A \rightarrow |0, 1\rangle_{l_1, l_2}. \quad (\text{A1})$$

A pure state $|\psi\rangle_A$ of the qubit system can be expressed in such a computational basis as

$$|\psi\rangle_A = \alpha |1, 0\rangle_{l_1, l_2} + \beta |0, 1\rangle_{l_1, l_2} \quad (\text{A2})$$

$$= \alpha |H\rangle_A + \beta |V\rangle_A, \quad (\text{A3})$$

where $\alpha, \beta \in \mathbb{C}$ and $|\alpha|^2 + |\beta|^2 = 1$. The bipartite entangled state Ψ_{AB}^+ is expressed as $\Psi_{AB}^+ = |\Psi^+\rangle\langle\Psi^+|_{AB}$ where $|\Psi^+\rangle_{AB} = \frac{1}{\sqrt{2}}(|HH\rangle_{AB} + |VV\rangle_{AB})$.

Appendix B: Two-qubit states

The maximally entangled states for the two-qubit systems can be expressed as

$$\begin{aligned} \Phi_{AB}^\pm &:= |\Phi^\pm\rangle\langle\Phi^\pm|_{AB} \\ \Psi_{AB}^\pm &:= |\Psi^\pm\rangle\langle\Psi^\pm|_{AB} \end{aligned} \quad (\text{B1})$$

where $|\Psi\rangle_{AB}^\pm$ and $|\Phi\rangle_{AB}^\pm$ are defined as

$$|\Psi\rangle_{AB}^\pm := \frac{1}{\sqrt{2}} \left(|00\rangle_{AB} \pm |11\rangle_{AB} \right), \quad (\text{B2})$$

$$|\Phi\rangle_{AB}^\pm := \frac{1}{\sqrt{2}} \left(|01\rangle_{AB} \pm |10\rangle_{AB} \right). \quad (\text{B3})$$

Following from Eq. (3), a two-qubit isotropic state can be expressed as

$$\rho_{AB}^I(p, 2) = \frac{1}{3}(4p - 1)\Psi_{AB}^+ + \frac{4}{3}(1 - p)\frac{\mathbb{1}_{AB}}{4}. \quad (\text{B4})$$

Similarly, following from Eq. (5), a two-qubit Werner state can be expressed as

$$\rho_{AB}^W(p(\lambda), 2) = \lambda\Psi_{AB}^- + (1 - \lambda)\frac{\mathbb{1}_{AB}}{4}, \quad (\text{B5})$$

where $\lambda \in [-1/3, 1]$.

⁷ An optical mode of the photon is defined by the state space consisting of a superposition of number states.

Appendix C: Two qubit Bell measurement on isotropic states

Let there be a measurement station that performs Bell measurement on the halves of two-qubit isotropic states $\rho_{A_1 A'_1}^I(p'(\lambda), 2)$ and $\rho_{B_1 B'_1}^I(p'(\lambda), 2)$, where

$$\rho_{AB}^I(p'(\lambda), 2) := \lambda \Psi_{AB}^+ + (1 - \lambda) \frac{\mathbb{1}_{AB}}{4}. \quad (C1)$$

We call λ the visibility of the isotropic state $\rho_{AB}^I(p'(\lambda), 2)$. Let the success probability of a Bell measurement be q . We denote the action of the noisy Bell measurement channel as

$$\begin{aligned} & \mathcal{E}_{A'_1 B'_1 \rightarrow I_A I'_A I_B I'_B} \left(\rho_{A_1 A'_1}^I(p'(\lambda), 2) \otimes \rho_{B_1 B'_1}^I(p'(\lambda), 2) \right) \\ = & \frac{\lambda^2 q}{4} \left[\Psi_{A_1 B_1}^- \otimes |00\rangle\langle 00|_{I_A I_B} \right. \\ & + \Psi_{A_1 B_1}^+ \otimes |11\rangle\langle 11|_{I_A I_B} + \Phi_{A_1 B_1}^- \otimes |22\rangle\langle 22|_{I_A I_B} \\ & \left. + \Phi_{A_1 B_1}^+ \otimes |33\rangle\langle 33|_{I_A I_B} \right] \otimes |00\rangle\langle 00|_{I'_A I'_B} \\ & + (1 - \lambda^2) q \frac{\mathbb{1}_{A_1 B_1}}{4} \otimes \frac{1}{4} \sum_{i=0}^3 |ii\rangle\langle ii|_{I_A I_B} \otimes |00\rangle\langle 00|_{I'_A I'_B} \\ & + (1 - q) \frac{\mathbb{1}_{A_1 B_1}}{4} \otimes |\perp\rangle\langle \perp|_{I_A I_B} \otimes |11\rangle\langle 11|_{I'_A I'_B}. \quad (C2) \end{aligned}$$

The flag state $|11\rangle\langle 11|_{I'_A I'_B}$ indicates error in the Bell measurement with a probability $(1 - q)$ and the state $\frac{\mathbb{1}_{A_1 B_1}}{4}$ is left on $\mathcal{H}_{A_1 B_1}$. The flag state $|00\rangle\langle 00|_{I'_A I'_B}$ indicates a successful Bell measurement with probability q . If error corrections are possible post-Bell measurement, then from a single use of repeater we have the state

$$\rho_{AB}^W(p(\lambda^2), 2) = \lambda^2 \Psi_{AB}^+ + (1 - \lambda^2) \frac{\mathbb{1}_{AB}}{4} \quad (C3)$$

with a probability q .

Appendix D: Actions of some quantum channels

1. The qubit depolarizing channel

The action of a qubit depolarizing channel [194] on the qubit density operator ρ_A is given by

$$\mathcal{D}_{A \rightarrow B}(\rho_A) = (1 - p) \rho_B + p \frac{\mathbb{1}_B}{2}, \quad (D1)$$

where $p \in [0, \frac{4}{3}]$ is the channel parameter and $\mathbb{1}_B$ is the identity operator. In the formalism given by Kraus [195] and Choi [196] the effect of the channel can be defined

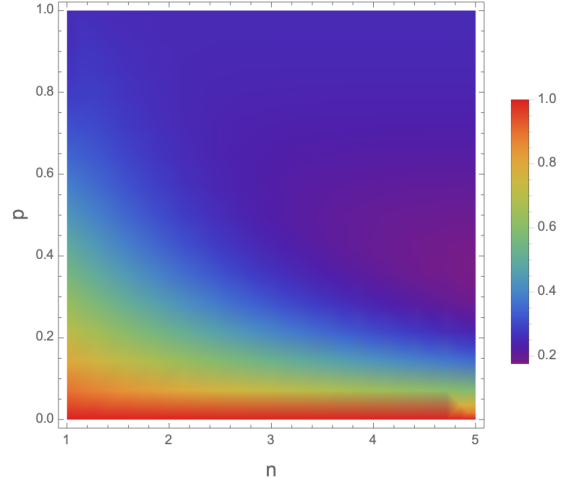


FIG. 23: In this figure, we plot the variation of η_d^n as a function of n and p . (Color online)

by the following operators [197],

$$\mathcal{K}_0 = \sqrt{1 - \frac{3p}{4}} \mathbb{1} \quad (D2)$$

$$\text{and } \mathcal{K}_i = \frac{\sqrt{p}}{2} \sigma_i \text{ with } i \in \{1, 2, 3\}, \quad (D3)$$

where σ_i are the Pauli matrices. The action of the depolarizing channel on each of the systems A and \bar{A} is given by,

$$\begin{aligned} & \mathcal{D}_{A \rightarrow B} \otimes \mathcal{D}_{\bar{A} \rightarrow \bar{B}} (\Psi_{AA}^+) \\ = & \sum_{i=0}^4 \sum_{j=0}^4 (\mathcal{K}_i \otimes \mathcal{K}_j) \Psi_{AA}^+ (\mathcal{K}_i \otimes \mathcal{K}_j)^\dagger \quad (D4) \end{aligned}$$

$$= (-1 + p)^2 \Psi_{BB}^+ + p(2 - p) \frac{\mathbb{1}_{B\bar{B}}}{4} \quad (D5)$$

Noting that $\mathbb{1}_{B\bar{B}}$ can be expressed as the sum of four maximally entangled states, we have the fidelity of the final state to the starting state as $\eta_d = 1 - \frac{3}{4} p(2 - p)$. Following the approach of [145] and applying the depolarizing channel n times, the final state after the evolution through the channel is

$$\rho_{B\bar{B}}^n = (\mathcal{D}_{A \rightarrow B} \otimes \mathcal{D}_{\bar{A} \rightarrow \bar{B}})^{\otimes n} (\Psi_{AA}^+).$$

This state $\rho_{B\bar{B}}^n$ has a fidelity with $\Psi_{B\bar{B}}^+$ given by

$$\eta_d^n = (1 - p)^{2n} - \frac{1}{4} (p - 2)p \left((n - 1)(1 - p)^{2(n-1)} + 1 \right), \quad (D6)$$

where it can be seen that $\eta_d^1 = \eta_d$. We plot in Fig. 23, the variation of η_d^n (using Eq. (D6)) as a function of the number of applications n of the depolarising channel and the depolarising channel parameter p .

2. The erasure channel

The action of a qubit erasure channel [198] on an input density operator ρ_A is given by

$$\mathcal{E}_{A \rightarrow B}(\rho_A) = \eta_e \rho_B + (1 - \eta_e) \text{Tr}[\rho_B] |e\rangle\langle e|_B. \quad (\text{D7})$$

The action of the erasure channel on the qubit system is such that it outputs the exact input state with probability η or with probability $1 - \eta$ replaces it with erasure state $|e\rangle$, where $|e\rangle$ is the vacuum state. The action of the channel on the maximally entangled state $\Psi_{A\bar{A}}^+$ in the two-qubit space $A\bar{A}$ is given by

$$\begin{aligned} \mathcal{E}_{A \rightarrow B} \otimes \mathcal{E}_{\bar{A} \rightarrow \bar{B}} (\Psi_{A\bar{A}}^+) \\ = \eta_e^2 \Psi_{B\bar{B}}^+ + (1 - \eta_e^2) \Psi_{B\bar{B}}^\perp, \end{aligned} \quad (\text{D8})$$

where

$$\begin{aligned} \Psi_{B\bar{B}}^\perp := \frac{\eta_e}{1 + \eta_e} \left(\frac{1}{2} \mathbb{1}_B \otimes |e\rangle\langle e|_{\bar{B}} + |e\rangle\langle e|_B \otimes \frac{1}{2} \mathbb{1}_{\bar{B}} \right) \\ + \frac{1 - \eta_e}{1 + \eta_e} |e\rangle\langle e|_B \otimes |e\rangle\langle e|_{\bar{B}} \end{aligned} \quad (\text{D9})$$

is a state orthogonal to $\Psi_{B\bar{B}}^+$.

Consider two sources creating pairs of entangled state Ψ^+ . The first and second source distributes the entangled pairs to node pairs (v_1, v_2) and (v_2, v_3) respectively via erasure channels. The node v_2 then performs a Bell measurement on its share of states. Assuming error correction is possible post-measurement, the node pair (v_1, v_3) share the state Ψ^+ with probability η_e^2 .

3. The qubit thermal channel

The action of a qubit thermal channel on the density operator ρ_A is given by

$$\mathcal{L}_{A \rightarrow B}^{\eta_g, n_g}(\rho_A) = \text{Tr}_E[U_{\eta_g}(\rho_A \otimes \rho_E) U_{\eta_g}^\dagger], \quad (\text{D10})$$

where ρ_E is the density operator of the environment given by

$$\rho_E = (1 - n_g) |0\rangle\langle 0|_E + n_g |1\rangle\langle 1|_E. \quad (\text{D11})$$

The qubit thermal channel is modelled by the interaction of a qubit system ρ_A with the environment ρ_E at a lossy beamsplitter having transmittance η_g (see Eq. (E5)). The evolution through the beamsplitter is via the unitary U_{η_g} expressed as

$$U_{\eta_g} = \begin{pmatrix} 1 & 0 & 0 & 0 \\ 0 & \sqrt{\eta_g} & \sqrt{1 - \eta_g} & 0 \\ 0 & -\sqrt{1 - \eta_g} & \sqrt{\eta_g} & 0 \\ 0 & 0 & 0 & 1 \end{pmatrix}. \quad (\text{D12})$$

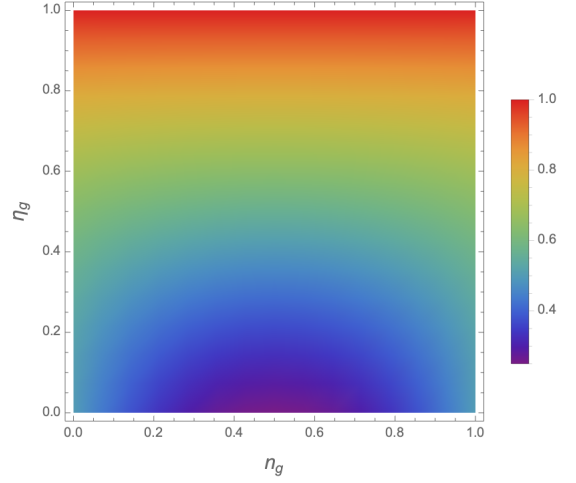


FIG. 24: In this figure, we plot the variation of η_t as a function of n_g and η_g . (Color online)

The Generalised Amplitude Damping Channel (GADC) is equivalent to the qubit thermal channel up to the reparameterization $\mathcal{A}_{A \rightarrow B}^{\eta_g, n_g}(\rho_A) \equiv \mathcal{L}_{A \rightarrow B}^{1 - \eta_g, n_g}(\rho_A)$ with $\eta_g \in [0, 1]$ and $n_g \in [0, 1]$. The effect of the thermal channel can be defined by the following Kraus operators in the standard basis

$$\widetilde{\mathcal{A}}_1 = \sqrt{1 - n_g}(|0\rangle\langle 0| + \sqrt{\eta_g}|1\rangle\langle 1|) \quad (\text{D13})$$

$$\widetilde{\mathcal{A}}_2 = \sqrt{(1 - \eta_g)(1 - n_g)}|0\rangle\langle 1| \quad (\text{D14})$$

$$\widetilde{\mathcal{A}}_3 = \sqrt{n_g}(\sqrt{\eta_g}|0\rangle\langle 0| + |1\rangle\langle 1|) \quad (\text{D15})$$

$$\widetilde{\mathcal{A}}_4 = \sqrt{n_g(1 - \eta_g)}|1\rangle\langle 0|. \quad (\text{D16})$$

The action of the thermal channel on each of the systems A and \bar{A} is given by,

$$\begin{aligned} \tau_{B\bar{B}}^{\eta_g, n_g} &:= \mathcal{L}_{A \rightarrow B}^{\eta_g, n_g} \otimes \mathcal{L}_{\bar{A} \rightarrow \bar{B}}^{\eta_g, n_g} (\Psi_{A\bar{A}}^+) \\ &= \sum_{i=0}^4 \sum_{j=0}^4 (\widetilde{\mathcal{A}}_i \otimes \widetilde{\mathcal{A}}_j) (\Psi_{A\bar{A}}^+) (\widetilde{\mathcal{A}}_i \otimes \widetilde{\mathcal{A}}_j)^\dagger \\ &= \eta_g \Psi_{B\bar{B}}^+ \\ &\quad + (1 - \eta_g)(n_g - 1) \left(n_g(1 - \eta_g) - 1 \right) |00\rangle\langle 00|_{B\bar{B}} \\ &\quad + n_g(-1 + \eta_g) \left(n_g(-1 + \eta_g) - \eta_g \right) |11\rangle\langle 11|_{B\bar{B}} \\ &\quad + n_g(1 - n_g)(1 - \eta_g)^2 (|01\rangle\langle 01|_{B\bar{B}} + |10\rangle\langle 10|_{B\bar{B}}). \end{aligned} \quad (\text{D17})$$

The state $\tau_{B\bar{B}}^{\eta_g, n_g}$ has a fidelity with $\Psi_{B\bar{B}}^+$ given by

$$\eta_t = \frac{1}{2}(1 + \eta_g^2) + n_g(n_g - 1)(1 - \eta_g)^2. \quad (\text{D18})$$

We plot in Fig 24, the variation of η_t as a function of the channel parameters η_g and n_g .

Appendix E: The atmospheric channel

The losses in the transmission of optical signals via an optical fiber are greater than that for free space transmission. In the vacuum space above the earth's atmosphere, the losses are nearly negligible. The non-birefringent nature of the atmosphere causes negligible change to the polarization state of the photons passing through it. These observations motivate the use of space and satellite technologies in establishing an entanglement distribution network using such channels. We observe in Fig. 25, that the losses in the satellite-based free-space channel is much less compared to fiber-based channels for distances greater than 70 km.

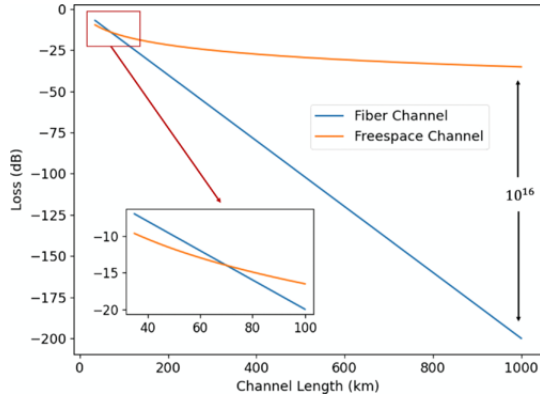


FIG. 25: The comparison of losses in fiber and free-space channels as a function of channel length as discussed in [98]. It is observed that the free-space channel is advantageous for distances over 70 km. (Color online)

The network architecture should be a hybrid satellite-optical fiber based model with ground-based global nodes at different geographical locations that are connected to different local nodes at small distances via optical fibers. These global nodes will be connected to the inter-satellite network. This architecture can in principle be extended to deep space allowing the possibility of sharing entanglement between nodes on Earth and the moon.

The factors affecting the transmission of optical signals between a satellite and a ground station are analyzed next. We obtain the efficiency in transmission ξ_{eff} considering losses due to (a) inefficiencies in transmitting (ξ_t) and receiving systems (ξ_r), (b) beam diffraction (ξ_d), (c) air turbulence (ξ_{at}), (d) mispointing (ξ_p) and (e) atmospheric absorption (ξ_{as}). The total transmittance is given by

$$\xi_{\text{eff}} = \xi_t \xi_r \xi_d \xi_{at} \xi_p \xi_{as}. \quad (\text{E1})$$

The diffraction of an optical beam depends on the beam's spatial mode, wavelength and aperture of the telescope. Assuming a Gaussian beam from the source with a waist radius of ω_0 , the radius at a distance z is given by $\omega_d(z) =$

$\omega_0 \sqrt{1 + (z/z_R)^2}$ with z_R being the Rayleigh range. If the aperture radius of the telescope is r , then the receiving efficiency is given by [98]

$$\xi_d = 1 - \exp\left\{-\frac{2r^2}{\omega_d^2}\right\}. \quad (\text{E2})$$

The turbulence in the atmosphere induces inhomogeneity in the refractive index which changes the direction of the propagating beam. It was shown in [199] that large-scale turbulence causes beam deflection while small-scale turbulence induces beam broadening. At the receiver end, it was shown in [200] that the average long-term accumulation of the moving spots shows a Gaussian distribution with an equivalent spot radius of $\omega_{at}(z) = \omega_d(z) \sqrt{1 + 1.33\sigma_R^2 \Lambda^{5/6}}$, where σ_R^2 is the Rytov variance for plane wave and Λ is the Fresnel ratio of the beam at the receiver. The receiving efficiency is given by

$$\xi_{at} = 1 - \exp\left\{-\frac{2r^2}{\omega_{at}^2}\right\}. \quad (\text{E3})$$

Next, for the satellite moving at a high speed a high-precision and high-bandwidth acquisition, pointing and tracking (APT) system generally consisting of coarse and fine tracking systems is required. A combination of closed-loop coarse tracking having a large field of view along with fine tracking having a small field of view is generally used. The pointing error induces a spot jitter with the instantaneous spot following a Rice intensity distribution. It was shown in [201] that the pointing efficiency is given by

$$\xi_p = 1 - \frac{\omega_{at}^2}{\omega_{at}^2 + 4\sigma_p^2}, \quad (\text{E4})$$

where σ_p is the variance of the Gaussian pointing probability distribution.

Inserting Eq. (E2), Eq. (E3), and Eq. (E4) in Eq. (E1) and imposing the condition that $\sigma_p = \eta \omega_{at}$ we obtain

$$\xi_{\text{eff}} = \frac{\eta^2 \xi_{as} \xi_r \xi_t}{\eta^2 + 0.25} \left(1 - \exp\left\{-\frac{2r^2 z_R^2}{w^2(z^2 + z_R^2)}\right\} \right) \left(1 - \exp\left\{-\frac{2r^2}{w^2(1.33\Lambda^{5/6}\sigma_R^2 + 1)(\frac{z^2}{z_R^2} + 1)}\right\} \right) \quad (\text{E5})$$

Consider a 780 nm source with a beam waist radius ω_0 of 0.0021 m and quality factor 1. The source has a Rayleigh length (z_R) = 17.8 m. Let the channel have Rytov variance (σ_R) = 0.1, and the Fresnel ratio of the beam at the receiver end is (Λ) = 0.1. Let the efficiency of the receiving unit be (ξ_r) = 0.99, that of the transmitting source be (ξ_t) = 0.99. Also let the probability of successful transmission after atmospheric absorption be (ξ_{as}) = 0.5. Assuming $\eta = 0.95$, we plot in Fig. 26 the transmission probability through the atmosphere as a function of the radius of the receiving telescope for dif-

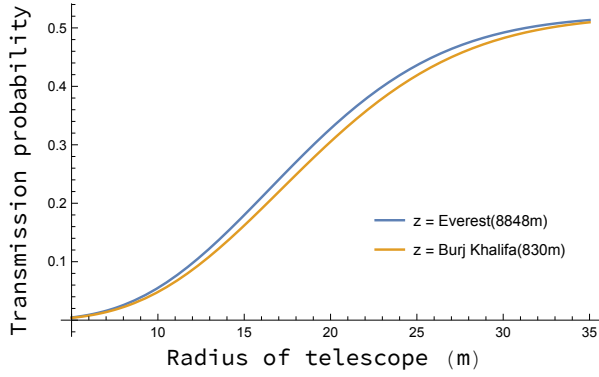


FIG. 26: In this figure, we plot the variation of the transmission probability as a function of the radius of the telescope for different receiving station altitudes.

For this, we have considered a 780 nm source with $\omega_0 = 0.0021$ and quality factor 1. We have set $z_R = 17.8$, $\sigma_R = 0.1$, $\Lambda = 0.1$, $\xi_r = 0.99$, $\xi_t = 0.99$, $\xi_{as} = 0.5$ and $\eta = 0.95$. (Color online)

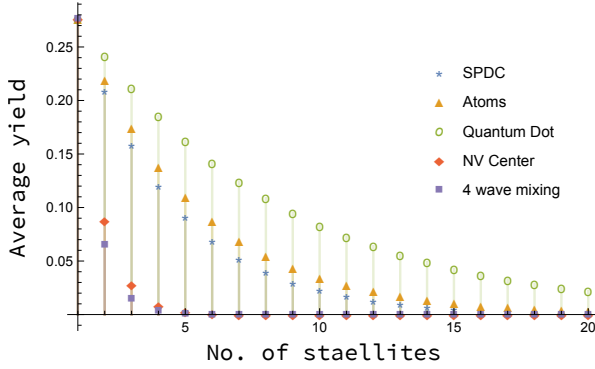


FIG. 27: In this figure, we plot the average yield ξ_{avg} (see Eq. (51)) as a function of the number of satellites

in the network for different single photon source architectures. The single photon source architectures have the source efficiencies (a) $\eta_s = 0.84$ (SPDC [166]) (b) $\eta_s = 0.88$ (Atoms [165]) (c) $\eta_s = 0.97$ (Quantum Dots [164]) (d) $\eta_s = 0.35$ (NV Center [202]) and (e) $\eta_s = 0.26$ (4 wave mixing [203]). For this, we set $L = l_B + l_M = 10$ km, $s = 1$, $p = 0.1$, $\eta_e = 0.95$, $\eta_1 = 0.5$, $n_1 = 0.5$, $\alpha = 1/22$ km $^{-1}$. (Color online)

ferent altitudes.

Appendix F: Entanglement distribution across cities

We plot in Fig. 27 the variation of ξ_{avg} as a function of the number of satellites in the network for different currently available single photon sources.

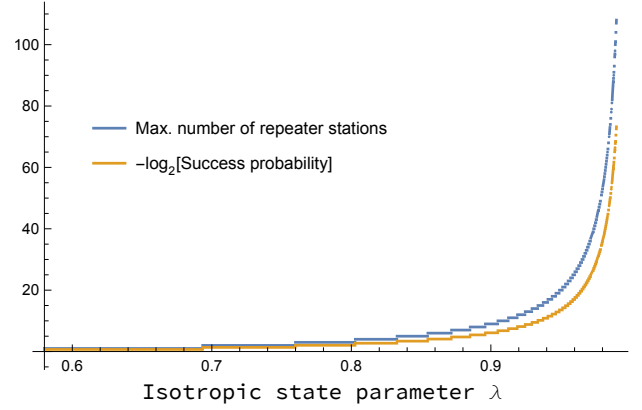


FIG. 28: In this figure, we plot (a) the maximum allowed number of relay stations between Alice and Bob (shown in blue) and (b) $\log(\text{success probability})$ (in yellow) for the state $\rho_{AB}^I(p(\lambda^{n+1}), 2)$ to be useful for teleportation protocol. (Color online)

Appendix G: Limitations of linear repeater networks

Let us consider two distant parties, Alice and Bob requiring to share an entangled state using an entanglement swapping protocol as described in Sec. III. Assuming that there are n repeater stations between Alice and Bob, they share the isotropic state

$$\rho_{AB}^I(p(\lambda^{n+1}), 2) = \lambda^{n+1} \Psi_{AB}^+ + \frac{1}{4}(1 - \lambda^{n+1}) \mathbb{1}_{AB} \quad (\text{G1})$$

of visibility λ^{n+1} with a probability q^n . In the following propositions, we present the bound on the number of virtual nodes in the network such that the state $\rho_{AB}^I(p(\lambda^{n+1}), 2)$ (a) is useful for teleportation, (b) can violate the Bell-CHSH inequality and (c) is entangled.

Proposition 3. *The state $\rho_{AB}^I(p(\lambda^{n+1}), 2)$ can be used to perform teleportation protocol with a success probability q^n when*

$$n < \lfloor \frac{\log(3)}{\log(1/\lambda)} - 1 \rfloor. \quad (\text{G2})$$

Proof. Let us have u_k as the eigenvalues of the matrix $T^\dagger T$ where the T matrix is formed by the elements $t_{nm} = \text{Tr}[\rho_{AB}^I(p(\lambda^{n+1}), 2) \sigma_n \otimes \sigma_m]$ where σ_j denotes the Pauli matrices. We then define the quantity $N(\rho_{AB}) = \sum_{k=1}^3 \sqrt{u_k}$. The state $\rho_{AB}^I(p(\lambda^{n+1}), 2)$ is useful for teleportation for values of $N(\rho_{AB})$ greater than 1 [59]. This then implies $n < \lfloor \frac{\log(3)}{\log(1/\lambda)} - 1 \rfloor$. \square

We plot in Fig. 28 the maximum number of repeater stations that can be allowed for a given value of λ and setting $q = 0.625$ [204] to successfully implement a teleportation protocol.

Proposition 4. *The state $\rho_{AB}^I(p(\lambda^{n+1}), 2)$ can violate the Bell-CHSH inequality with a success probability q^n*

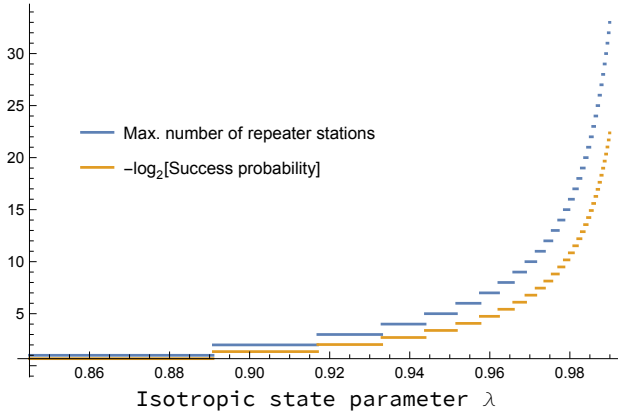


FIG. 29: In this figure, we plot (a) the maximum allowed number of relay stations between Alice and Bob (shown in blue) and (b) $\log(\text{success probability})$ (in yellow) for the state $\rho_{AB}^I(p(\lambda^{n+1}), 2)$ to violate the Bell-CHSH inequality. (Color online)

when

$$n < \lfloor \frac{\log(2)}{2\log(1/\lambda)} - 1 \rfloor. \quad (\text{G3})$$

Proof. Let us have u_i, u_j be the two largest eigenvalues of the matrix $T^\dagger T$ where the T matrix is formed by the elements $t_{nm} = \text{Tr}[\rho_{AB}^I(p(\lambda^{n+1}), 2) \sigma_n \otimes \sigma_m]$ where σ_j denotes the Pauli matrices. We then define the quantity $M(\rho_{AB}) = u_i + u_j$. The state $\rho_{AB}^I(p(\lambda^{n+1}), 2)$ is Bell-CHSH nonlocal for values of $M(\rho_{AB})$ greater than 1 [205]. This then implies $n < \lfloor \frac{\log(2)}{2\log(1/\lambda)} - 1 \rfloor$. \square

We plot in Fig. 29 the maximum number of repeater stations that can be allowed for a given value of λ and setting $q = 0.625$ [204] such that the state shared by the end nodes can violate the Bell-CHSH inequality.

Proposition 5. *The state $\rho_{AB}^I(p(\lambda^{n+1}), 2)$ remains entangled with a success probability q^n when*

$$n < \lfloor \frac{\log 3}{\log(1/\lambda)} - 1 \rfloor. \quad (\text{G4})$$

Proof. The concurrence of the state $\rho_{AB}^I(p(\lambda^{n+1}), 2)$ is given by $\max\{0, \lambda_1^e - \lambda_2^e - \lambda_3^e - \lambda_4^e\}$ [206] where the λ_s^e are the eigenvalues of $\rho_{AB}^I(p(\lambda^{n+1}), 2)(\rho_{AB}^I(p(\lambda^{n+1}), 2))_f$ in descending order. The spin flipped density matrix is given by $(\rho_{AB}^I(p(\lambda^{n+1}), 2))_f = (\sigma_y \otimes \sigma_y) \rho_{AB}^I(p(\lambda^{n+1}), 2) (\sigma_y \otimes \sigma_y)$. The state is entangled when the concurrence is greater than zero. This requires $n < \frac{\log 3}{\log(1/\lambda)} - 1$. \square

We plot in Fig. 30 the maximum number of repeater stations that can be allowed for a given value of λ and setting $q = 0.625$ [204] such that the end nodes can share an entangled state. It is observed that the number of allowed repeater stations in the network depends on the

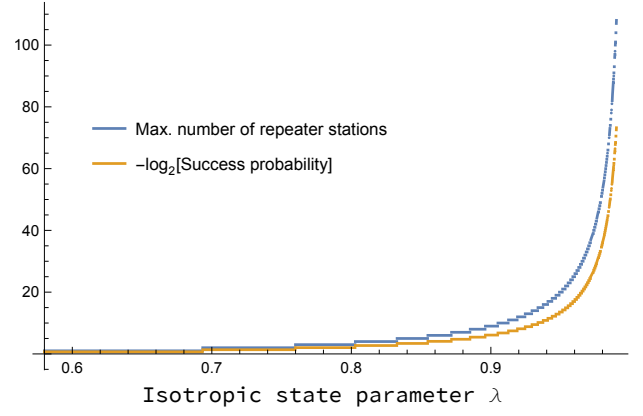


FIG. 30: In this figure, we plot (a) the maximum allowed number of relay stations between Alice and Bob (shown in blue) and (b) $\log(\text{success probability})$ (in yellow) for the state $\rho_{AB}^I(p(\lambda^{n+1}), 2)$ to remain entangled. (Color online)

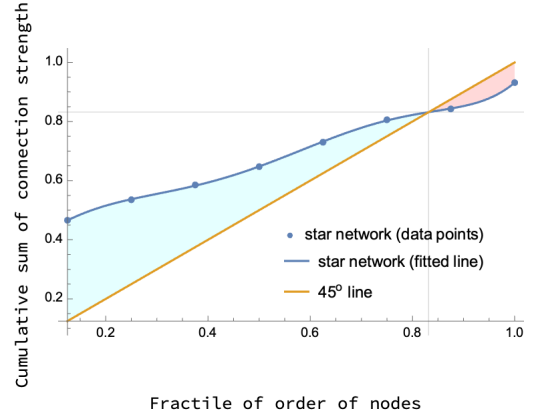


FIG. 31: In this figure, we plot (a) the cumulative sum of connection strength of the edges and (b) the 45 degree line with the fractiles of the order of nodes along the x-axis for the star network in Fig. 9. The ratio of the area enclosed by (a) and (b) provides the sparsity index of the network. The shaded area in cyan and red provides advantages and disadvantages over a star network with equal edge weights. (Color online)

information processing task that the network is executing. The number of allowed repeater stations increases with the increase in λ . Furthermore, the success probability of the information processing task decreases with an increase in the number of allowed repeater stations.

Appendix H: Sparsity index of a star network

Consider a star network with 8 nodes as shown in Fig. 9. The node v_1 is the hub node and nodes v_2 to v_8 are the leaf nodes. We plot in Fig. 31 the cumulative sum of the connection strength of the edges and the 45

degree line. The sparsity index of the star network is given by 1.22928. The sparsity index of other networks can be obtained using a similar approach.

Appendix I: Analysis of time-varying quantum networks

In general, the network parameters i.e., the number of nodes, edges, and edge weights may change with time. Let us denote such a time-varying network as $\mathcal{N}(G(\mathbb{V}(t), \mathbb{E}(t)))$. We say that two nodes v_i and v_j of a time-varying network are connected in the time interval $[t_1, t_2]$ if $\exists e_{ij} \in \mathbb{E}(t)$ with $p_{ij} \geq p_*$ $\forall t \in [t_1, t_2]$. In the following example, we present the variation of link sparsity with time for the time-varying network shown in Fig. 32.

Example 4. Consider a network $\mathcal{N}(G(\mathbb{V}(t), \mathbb{E}(t)))$ whose vertices and edges are evolving in time as shown in Fig. 32. We assume that for $e_{ij} \in \mathbb{E}(t)$,

$$p_{ij}(t+1) := \begin{cases} we^{-kt} p_{ij}(t) & \text{for } we^{-kt} p_{ij}(t) > p_*, \\ 0 & \text{otherwise,} \end{cases} \quad (\text{II})$$

where $w = 0.9, p_* = 0.05, k = 0.3 \text{ sec}^{-1}$ and $t \in [1, 4]$.

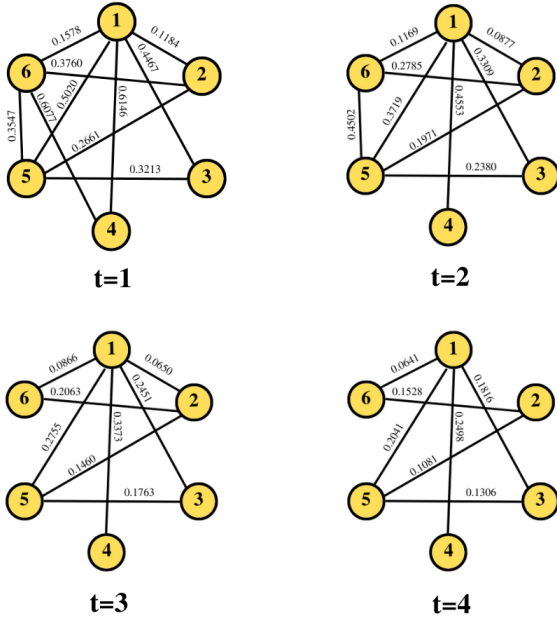


FIG. 32: We present a time varying mesh network with 6 nodes as a series of 4 static graphs. We consider the network topology at times $t \in \{1, 2, 3, 4\}$. In this network, the edges e_{ij} connecting nodes v_i and v_j denote the success probabilities p_{ij} of transferring some resource between the v_i and v_j . The success probability p_{ij} evolves in time following Eq. (II). (Color online)

For such a network, we have the variation of the link sparsity with time as

t (sec)	1	2	3	4
$\Upsilon(\mathcal{N})$	0.4445	0.5	0.5556	0.6112

TABLE II: Link sparsity for time-evolving graph

We observe from Table II that for the network shown in Fig 32, the link sparsity increases with time and the network becomes less robust.

- [1] Jonathan P Dowling and Gerard J Milburn, "Quantum technology: the second quantum revolution," *Philosophical Transactions of the Royal Society of London. Series A: Mathematical, Physical and Engineering Sciences* **361**, 1655–1674 (2003).
- [2] H Jeff Kimble, "The quantum internet," *Nature* **453**, 1023–1030 (2008).
- [3] Stephanie Wehner, David Elkouss, and Ronald Hanson, "Quantum internet: A vision for the road ahead," *Science* **362**, eaam9288 (2018).
- [4] C. H. Bennett and G. Brassard, "Quantum cryptography: Public key distribution and coin tossing," *Proceedings of the IEEE International Conference on Computers, Systems and Signal Processing*, 175–179 (1984).
- [5] Artur K. Ekert, "Quantum cryptography based on Bell's theorem," *Physical Review Letters* **67**, 661–663 (1991).
- [6] Antonio Acín, Nicolas Brunner, Nicolas Gisin, Serge Massar, Stefano Pironio, and Valerio Scarani, "Device-independent security of quantum cryptography against collective attacks," *Physical Review Letters* **98**, 230501 (2007).
- [7] Renato Renner, "Security of quantum key distribution," *International Journal of Quantum Information* **6**, 1–127 (2008).
- [8] Jonathan Barrett, Roger Colbeck, and Adrian Kent, "Memory Attacks on Device-Independent Quantum Cryptography," *Physical Review Letters* **110**, 010503 (2013).
- [9] Marco Lucamarini, Zhiliang L Yuan, James F Dynes, and Andrew J Shields, "Overcoming the rate–distance limit of quantum key distribution without quantum repeaters," *Nature* **557**, 400–403 (2018).
- [10] Rotem Arnon-Friedman, Frédéric Dupuis, Omar Fawzi, Renato Renner, and Thomas Vidick, "Practical device-independent quantum cryptography via entropy accumulation," *Nature communications* **9**, 459 (2018).
- [11] Siddhartha Das, "Bipartite Quantum Interactions: Entangling and Information Processing Abilities," (2019), arXiv:1901.05895.
- [12] Feihu Xu, Xiongfeng Ma, Qiang Zhang, Hoi-Kwong Lo, and Jian-Wei Pan, "Secure quantum key distribution with realistic devices," *Reviews of Modern Physics* **92**, 025002 (2020).
- [13] Siddhartha Das, Stefan Bäuml, Marek Winczewski, and Karol Horodecki, "Universal limitations on quantum key distribution over a network," *Physical Review X* **11**, 041016 (2021).
- [14] Peter W Shor, "Algorithms for quantum computation: discrete logarithms and factoring," in *Proceedings 35th annual symposium on foundations of computer science* (Ieee, 1994) pp. 124–134.
- [15] Richard Jozsa, "Entanglement and quantum computation," (1997), arXiv quant-ph/9707034.
- [16] Lov K Grover, "A fast quantum mechanical algorithm for database search," in *Proceedings of the twenty-eighth annual ACM symposium on Theory of computing* (1996) pp. 212–219.
- [17] Emanuel Knill, Raymond Laflamme, and Gerald J Milburn, "A scheme for efficient quantum computation with linear optics," *Nature* **409**, 46–52 (2001).
- [18] Andrew M Childs, Richard Cleve, Enrico Deotto, Edward Farhi, Sam Gutmann, and Daniel A Spielman, "Exponential algorithmic speedup by a quantum walk," in *Proceedings of the thirty-fifth annual ACM symposium on Theory of computing* (2003) pp. 59–68.
- [19] Samuel L. Braunstein and Peter van Loock, "Quantum information with continuous variables," *Reviews of Modern Physics* **77**, 513–577 (2005).
- [20] Nicolas C. Menicucci, Peter van Loock, Mile Gu, Christian Weedbrook, Timothy C. Ralph, and Michael A. Nielsen, "Universal Quantum Computation with Continuous-Variable Cluster States," *Physical Review Letters* **97**, 110501 (2006).
- [21] Scott Aaronson and Alex Arkhipov, "The computational complexity of linear optics," in *Proceedings of the forty-third annual ACM symposium on Theory of computing* (2011) pp. 333–342.
- [22] J Ignacio Cirac, AK Ekert, Susana F Huelga, and Chiara Macchiavello, "Distributed quantum computation over noisy channels," *Physical Review A* **59**, 4249 (1999).
- [23] Matthias Fitz, Nicolas Gisin, and Ueli Maurer, "Quantum Solution to the Byzantine Agreement Problem," *Physical Review Letters* **87**, 217901 (2001).
- [24] Robert Raussendorf and Hans J. Briegel, "A One-Way Quantum Computer," *Physical Review Letters* **86**, 5188–5191 (2001).
- [25] Robert Beals, Stephen Brierley, Oliver Gray, Aram W Harrow, Samuel Kutin, Noah Linden, Dan Shepherd, and Mark Stather, "Efficient distributed quantum computing," *Proceedings of the Royal Society A: Mathematical, Physical and Engineering Sciences* **469**, 20120686 (2013).
- [26] Yuan Liang Lim, Almut Beige, and Leong Chuan Kwek, "Repeat-until-success Linear Optics Distributed Quantum Computing," *Physical Review Letters* **95**, 030505 (2005).
- [27] Xiao Liu, Xiao-Min Hu, Tian-Xiang Zhu, Chao Zhang, Yi-Xin Xiao, Jia-Le Miao, Zhong-Wen Ou, Bi-Heng Liu, Zong-Quan Zhou, Chuan-Feng Li, and Guang-Can Guo, "Distributed quantum computing over 7.0 km," (2023), arXiv:2307.15634.
- [28] Andrew M Childs, "Secure assisted quantum computation," (2001), arXiv quant-ph/0111046.
- [29] Vittorio Giovannetti, Seth Lloyd, and Lorenzo Maccone, "Quantum private queries," *Physical Review Letters* **100**, 230502 (2008).
- [30] Anne Broadbent, Joseph Fitzsimons, and Elham Kashefi, "Universal blind quantum computation," in *2009 50th annual IEEE symposium on foundations of computer science* (IEEE, 2009) pp. 517–526.
- [31] Siddhartha Das and George Siopsis, "Practically secure quantum position verification," *New Journal of Physics* **23**, 063069 (2021).
- [32] J. J. Bollinger, Wayne M. Itano, D. J. Wineland, and D. J. Heinzen, "Optimal frequency measurements with maximally correlated states," *Physical Review A* **54**, R4649–R4652 (1996).
- [33] Vittorio Giovannetti, Seth Lloyd, and Lorenzo Maccone, "Quantum-enhanced measurements: beating the standard quantum limit," *Science* **306**, 1330–1336

- (2004).
- [34] Vittorio Giovannetti, Seth Lloyd, and Lorenzo Maccone, “Quantum Metrology,” *Physical Review Letters* **96**, 010401 (2006).
 - [35] Dmitry Budker and Michael Romalis, “Optical magnetometry,” *Nature physics* **3**, 227–234 (2007).
 - [36] Jacob M Taylor, Paola Cappellaro, Lilian Childress, Liang Jiang, Dmitry Budker, PR Hemmer, Amir Yacoby, Ronald Walsworth, and MD Lukin, “High-sensitivity diamond magnetometer with nanoscale resolution,” *Nature Physics* **4**, 810–816 (2008).
 - [37] C. L. Degen, F. Reinhard, and P. Cappellaro, “Quantum sensing,” *Reviews of Modern Physics* **89**, 035002 (2017).
 - [38] Johannes Jakob Meyer, Sumeet Khatri, Daniel Stilck França, Jens Eisert, and Philippe Faist, “Quantum metrology in the finite-sample regime,” (2023), arXiv:2307.06370.
 - [39] Isaac L. Chuang, “Quantum Algorithm for Distributed Clock Synchronization,” *Physical Review Letters* **85**, 2006–2009 (2000).
 - [40] Richard Jozsa, Daniel S. Abrams, Jonathan P. Dowling, and Colin P. Williams, “Quantum Clock Synchronization Based on Shared Prior Entanglement,” *Physical Review Letters* **85**, 2010–2013 (2000).
 - [41] Vittorio Giovannetti, Seth Lloyd, and Lorenzo Maccone, “Quantum-enhanced positioning and clock synchronization,” *Nature* **412**, 417–419 (2001).
 - [42] Charles H. Bennett and Stephen J. Wiesner, “Communication via one-and two-particle operators on Einstein-Podolsky-Rosen states,” *Physical Review Letters* **69**, 2881–2884 (1992).
 - [43] Charles H Bennett, Gilles Brassard, Sandu Popescu, Benjamin Schumacher, John A Smolin, and William K Wootters, “Purification of noisy entanglement and faithful teleportation via noisy channels,” *Physical Review Letters* **76**, 722 (1996).
 - [44] Benjamin Schumacher, “Sending entanglement through noisy quantum channels,” *Physical Review A* **54**, 2614–2628 (1996).
 - [45] Klaus Mattle, Harald Weinfurter, Paul G. Kwiat, and Anton Zeilinger, “Dense Coding in Experimental Quantum Communication,” *Physical Review Letters* **76**, 4656–4659 (1996).
 - [46] S. J. van Enk, J. I. Cirac, and P. Zoller, “Ideal Quantum Communication over Noisy Channels: A Quantum Optical Implementation,” *Physical Review Letters* **78**, 4293–4296 (1997).
 - [47] Sougato Bose, “Quantum Communication through an Unmodulated Spin Chain,” *Physical Review Letters* **91**, 207901 (2003).
 - [48] P. van Loock, T. D. Ladd, K. Sanaka, F. Yamaguchi, Kae Nemoto, W. J. Munro, and Y. Yamamoto, “Hybrid Quantum Repeater Using Bright Coherent Light,” *Physical Review Letters* **96**, 240501 (2006).
 - [49] Wei Zhang, Dong-Sheng Ding, Yu-Bo Sheng, Lan Zhou, Bao-Sen Shi, and Guang-Can Guo, “Quantum Secure Direct Communication with Quantum Memory,” *Physical Review Letters* **118**, 220501 (2017).
 - [50] Siddhartha Das, Stefan Bäuml, and Mark M. Wilde, “Entanglement and secret-key-agreement capacities of bipartite quantum interactions and read-only memory devices,” *Physical Review A* **101**, 012344 (2020).
 - [51] Eneet Kaur, Siddhartha Das, Mark M Wilde, and Andreas Winter, “Extendibility limits the performance of quantum processors,” *Physical Review Letters* **123**, 070502 (2019).
 - [52] M. K. Bhaskar, R. Riedinger, B. Machielse, D. S. Levonian, C. T. Nguyen, E. N. Knall, H. Park, D. Englund, M. Lončar, D. D. Sukachev, and M. D. Lukin, “Experimental demonstration of memory-enhanced quantum communication,” *Nature* **580**, 60–64 (2020).
 - [53] Jian Wei Cheong, Andri Pradana, and Lock Yue Chew, “Communication advantage of quantum compositions of channels from non-Markovianity,” *Physical Review A* **106**, 052410 (2022).
 - [54] X. S. Liu, G. L. Long, D. M. Tong, and Feng Li, “General scheme for superdense coding between multiparties,” *Physical Review A* **65**, 022304 (2002).
 - [55] Siddhartha Das and Mark M. Wilde, “Quantum rebound capacity,” *Physical Review A* **100**, 030302 (2019).
 - [56] Charles H. Bennett, Gilles Brassard, Claude Crépeau, Richard Jozsa, Asher Peres, and William K. Wootters, “Teleporting an unknown quantum state via dual classical and Einstein-Podolsky-Rosen channels,” *Physical Review Letters* **70**, 1895–1899 (1993).
 - [57] Dik Bouwmeester, Jian-Wei Pan, Klaus Mattle, Manfred Eibl, Harald Weinfurter, and Anton Zeilinger, “Experimental quantum teleportation,” *Nature* **390**, 575–579 (1997).
 - [58] Akira Furusawa, Jens Lykke Sørensen, Samuel L Braunstein, Christopher A Fuchs, H Jeff Kimble, and Eugene S Polzik, “Unconditional quantum teleportation,” *science* **282**, 706–709 (1998).
 - [59] Ryszard Horodecki, Michał Horodecki, and Paweł Horodecki, “Teleportation, Bell’s inequalities and inseparability,” *Physics Letters A* **222**, 21–25 (1996).
 - [60] P. van Loock and Samuel L. Braunstein, “Multipartite Entanglement for Continuous Variables: A Quantum Teleportation Network,” *Physical Review Letters* **84**, 3482–3485 (2000).
 - [61] S. Pironio, A. Acín, S. Massar, A. Boyer de la Giroday, D. N. Matsukevich, P. Maunz, S. Olmschenk, D. Hayes, L. Luo, T. A. Manning, and C. Monroe, “Random numbers certified by Bell’s theorem,” *Nature* **464**, 1021–1024 (2010).
 - [62] Roger Colbeck and Adrian Kent, “Private randomness expansion with untrusted devices,” *Journal of Physics A: Mathematical and Theoretical* **44**, 095305 (2011).
 - [63] Antonio Acín, Serge Massar, and Stefano Pironio, “Randomness versus nonlocality and entanglement,” *Physical Review Letters* **108**, 100402 (2012).
 - [64] Roger Colbeck and Renato Renner, “Free randomness can be amplified,” *Nature Physics* **8**, 450–453 (2012).
 - [65] Dong Yang, Karol Horodecki, and Andreas Winter, “Distributed private randomness distillation,” *Physical Review Letters* **123**, 170501 (2019).
 - [66] Erwin Schrödinger, “Discussion of probability relations between separated systems,” *Mathematical Proceedings of the Cambridge Philosophical Society* **31**, 555–563 (1935).
 - [67] Ryszard Horodecki, Paweł Horodecki, Michał Horodecki, and Karol Horodecki, “Quantum entanglement,” *Reviews of modern physics* **81**, 865 (2009).

- [68] Jian-Wei Pan, Zeng-Bing Chen, Chao-Yang Lu, Harald Weinfurter, Anton Zeilinger, and Marek Żukowski, “Multiphoton entanglement and interferometry,” *Reviews of Modern Physics* **84**, 777–838 (2012).
- [69] Siddhartha Das, Sumeet Khatri, and Jonathan P Dowling, “Robust quantum network architectures and topologies for entanglement distribution,” *Physical Review A* **97**, 012335 (2018).
- [70] Stefan Bäuml, Siddhartha Das, and Mark M. Wilde, “Fundamental Limits on the Capacities of Bipartite Quantum Interactions,” *Physical Review Letters* **121**, 250504 (2018).
- [71] Nicolai Friis, Giuseppe Vitagliano, Mehul Malik, and Marcus Huber, “Entanglement certification from theory to experiment,” *Nature Reviews Physics* **1**, 72–87 (2019).
- [72] Junjing Xing, Tianfeng Feng, Zhaobing Fan, Haitao Ma, Kishor Bharti, Dax Enshan Koh, and Yunlong Xiao, “Fundamental Limitations on Communication over a Quantum Network,” (2023), arXiv:2306.04983.
- [73] Sumeet Khatri, “On the design and analysis of near-term quantum network protocols using markov decision processes,” *AVS Quantum Science* **4** (2022).
- [74] John S Bell, “On the Einstein Podolsky Rosen paradox,” *Physics Physique Fizika* **1**, 195 (1964).
- [75] John F Clauser, Michael A Horne, Abner Shimony, and Richard A Holt, “Proposed experiment to test local hidden-variable theories,” *Physical Review Letters* **23**, 880 (1969).
- [76] Nicolas Brunner, Daniel Cavalcanti, Stefano Pironio, Valerio Scarani, and Stephanie Wehner, “Bell nonlocality,” *Review of Modern Physics* **86**, 419–478 (2014).
- [77] Armin Tavakoli, Alejandro Pozas-Kerstjens, Ming-Xing Luo, and Marc-Olivier Renou, “Bell nonlocality in networks,” *Reports on Progress in Physics* **85**, 056001 (2022).
- [78] Alain Aspect, Jean Dalibard, and Gérard Roger, “Experimental test of Bell’s inequalities using time-varying analyzers,” *Physical Review Letters* **49**, 1804 (1982).
- [79] B. Hensen, H. Bernien, A. E. Dréau, A. Reiserer, N. Kalb, M. S. Blok, J. Ruitenberg, R. F. L. Vermeulen, R. N. Schouten, C. Abellán, W. Amaya, V. Pruneri, M. W. Mitchell, M. Markham, D. J. Twitchen, D. Elkouss, S. Wehner, T. H. Taminiau, and R. Hanson, “Loophole-free Bell inequality violation using electron spins separated by 1.3 kilometres,” *Nature* **526**, 682–686 (2015).
- [80] Marissa Giustina, Marijn A. M. Versteegh, Sören Wengerowsky, Johannes Handsteiner, Armin Hochrainer, Kevin Phelan, Fabian Steinlechner, Johannes Kofler, Jan-Åke Larsson, Carlos Abellán, Waldimar Amaya, Valerio Pruneri, Morgan W. Mitchell, Jörn Beyer, Thomas Gerrits, Adriana E. Lita, Lynden K. Shalm, Sae Woo Nam, Thomas Scheidl, Rupert Ursin, Bernhard Wittmann, and Anton Zeilinger, “Significant-loophole-free test of bell’s theorem with entangled photons,” *Physical Review Letters* **115**, 250401 (2015).
- [81] Dipankar Home, Debashis Saha, and Siddhartha Das, “Multipartite Bell-type inequality by generalizing Wigner’s argument,” *Physical Review A* **91**, 012102 (2015).
- [82] Ming-Xing Luo, “Fully device-independent model on quantum networks,” *Physical Review Research* **4**, 013203 (2022).
- [83] Anders J. E. Bjerrum, Jonatan B. Brask, Jonas S. Neergaard-Nielsen, and Ulrik L. Andersen, “Proposal for a long-distance nonlocality test with entanglement swapping and displacement-based measurements,” *Physical Review A* **107**, 052611 (2023).
- [84] Alexander Streltsov, Uttam Singh, Himadri Shekhar Dhar, Manabendra Nath Bera, and Gerardo Adesso, “Measuring Quantum Coherence with Entanglement,” *Physical Review Letters* **115**, 020403 (2015).
- [85] Yao Yao, Xing Xiao, Li Ge, and C. P. Sun, “Quantum coherence in multipartite systems,” *Physical Review A* **92**, 022112 (2015).
- [86] Uttam Singh, Siddhartha Das, and Nicolas J. Cerf, “Partial order on passive states and hoffman majorization in quantum thermodynamics,” *Physical Review Research* **3**, 033091 (2021).
- [87] Alexander Streltsov, Gerardo Adesso, and Martin B. Plenio, “Colloquium: Quantum coherence as a resource,” *Review of Modern Physics* **89**, 041003 (2017).
- [88] Raju Valivarthi, Samantha I. Davis, Cristián Peña, Si Xie, Nikolai Lauk, Lautaro Narváez, Jason P. Allmaras, Andrew D. Beyer, Yewon Gim, Meraj Hussein, George Iskander, Hyunseong Linus Kim, Boris Korzh, Andrew Mueller, Mandy Rominsky, Matthew Shaw, Dawn Tang, Emma E. Wollman, Christoph Simon, Panagiotis Spentzouris, Daniel Oblak, Neil Sinclair, and Maria Spiropulu, “Teleportation systems toward a quantum internet,” *PRX Quantum* **1**, 020317 (2020).
- [89] Shuang Wang, Wei Chen, Zhen-Qiang Yin, Hong-Wei Li, De-Yong He, Yu-Hu Li, Zheng Zhou, Xiao-Tian Song, Fang-Yi Li, Dong Wang, Hua Chen, Yun-Guang Han, Jing-Zheng Huang, Jun-Fu Guo, Peng-Lei Hao, Mo Li, Chun-Mei Zhang, Dong Liu, Wen-Ye Liang, Chun-Hua Miao, Ping Wu, Guang-Can Guo, and Zheng-Fu Han, “Field and long-term demonstration of a wide area quantum key distribution network,” **22**, 21739–21756 (2014).
- [90] M Peev, C Pacher, R Alléaume, C Barreiro, J Bouda, W Boxleitner, T Debuisschert, E Diamanti, M Dianati, J F Dynes, S Fasel, S Fossier, M Fürst, J-D Gauthier, O Gay, N Gisin, P Grangier, A Happe, Y Hasani, M Hentschel, H Hübel, G Humer, T Länger, M Legré, R Lieger, J Lodewyck, T Lorünser, N Lütkenhaus, A Marhold, T Matyus, O Maurhart, L Monat, S Nauerth, J-B Page, A Poppe, E Querasser, G Ribordy, S Robyr, L Salvail, A W Sharpe, A J Shields, D Stucki, M Suda, C Tamas, T Themel, R T Thew, Y Thoma, A Treiber, P Trinkler, R Tualle-Broui, F Vannel, N Walenta, H Weier, H Weinfurter, I Wimberger, Z L Yuan, H Zbinden, and A Zeilinger, “The secoqc quantum key distribution network in Vienna,” *New Journal of Physics* **11**, 075001 (2009).
- [91] D Stucki, M Legré, F Buntschu, B Clausen, N Felber, N Gisin, L Henzen, P Junod, G Litzistorf, P Monbaron, L Monat, J-B Page, D Perroud, G Ribordy, A Rochas, S Robyr, J Tavares, R Thew, P Trinkler, S Ventura, R Voirol, N Walenta, and H Zbinden, “Long-term performance of the SwissQuantum quantum key distribution network in a field environment,” *New Journal of Physics* **13**, 123001 (2011).

- [92] Nissim Ofek, Andrei Petrenko, Reinier Heeres, Philip Reinhold, Zaki Leghtas, Brian Vlastakis, Yehan Liu, Luigi Frunzio, S. M. Girvin, L. Jiang, Mazhar Mirrahimi, M. H. Devoret, and R. J. Schoelkopf, “Extending the lifetime of a quantum bit with error correction in superconducting circuits,” *Nature* **536**, 441–445 (2016).
- [93] Siddhartha Das, Sumeet Khatri, George Siopsis, and Mark M. Wilde, “Fundamental limits on quantum dynamics based on entropy change,” *Journal of Mathematical Physics* **59** (2018), 10.1063/1.4997044.
- [94] Chenlu Wang, Xuegang Li, Huikai Xu, Zhiyuan Li, Junhua Wang, Zhen Yang, Zhenyu Mi, Xuehui Liang, Tang Su, Chuhong Yang, Guangyue Wang, Wenyan Wang, Yongchao Li, Mo Chen, Chengyao Li, Kehuan Linghu, Jiaxiu Han, Yingshan Zhang, Yulong Feng, Yu Song, Teng Ma, Jingning Zhang, Ruixia Wang, Peng Zhao, Weiyang Liu, Guangming Xue, Yirong Jin, and Haifeng Yu, “Towards practical quantum computers: Transmon qubit with a lifetime approaching 0.5 milliseconds,” *npj Quantum Information* **8**, 3 (2022).
- [95] Youngseok Kim, Andrew Eddins, Sajant Anand, Ken Xuan Wei, Ewout van den Berg, Sami Rosenblatt, Hasan Nayfeh, Yantao Wu, Michael Zaletel, Kristan Temme, and Abhinav Kandala, “Evidence for the utility of quantum computing before fault tolerance,” *Nature* **618**, 500–505 (2023).
- [96] Koji Azuma, Kiyoshi Tamaki, and Hoi-Kwong Lo, “All-photonic quantum repeaters,” *Nature Communications* **6**, 1–7 (2015).
- [97] Sebastian Ecker, Johannes Pseiner, Jorge Piris, and Martin Bohmann, “Advances in entanglement-based QKD for space applications,” (2022), arXiv:2210.02229.
- [98] Chao-Yang Lu, Yuan Cao, Cheng-Zhi Peng, and Jian-Wei Pan, “Micius quantum experiments in space,” *Reviews of Modern Physics* **94**, 035001 (2022).
- [99] Tonghua Liu, Shuo Cao, Sixuan Zhang, Hao Zheng, and Xiaobao Liu, “Satellite-based continuous-variable quantum key distribution under the Earth’s gravitational field,” *Quantum Information Processing* **21**, 397 (2022).
- [100] Eneet Kaur, Karol Horodecki, and Siddhartha Das, “Upper bounds on device-independent quantum key distribution rates in static and dynamic scenarios,” *Physical Review Applied* **18**, 054033 (2022).
- [101] H-J Briegel, Wolfgang Dür, Juan I Cirac, and Peter Zoller, “Quantum repeaters: the role of imperfect local operations in quantum communication,” *Physical Review Letters* **81**, 5932 (1998).
- [102] Francesco Buscemi, Siddhartha Das, and Mark M. Wilde, “Approximate reversibility in the context of entropy gain, information gain, and complete positivity,” *Physical Review A* **93**, 062314 (2016).
- [103] Yink Loong Len, Tuvia Gefen, Alex Retzker, and Jan Kolodyński, “Quantum metrology with imperfect measurements,” *Nature Communications* **13**, 6971 (2022).
- [104] Abhishek Sadhu and Siddhartha Das, “Testing of quantum nonlocal correlations under constrained free will and imperfect detectors,” *Physical Review A* **107**, 012212 (2023).
- [105] Christopher A Fuchs and Asher Peres, “Quantum-state disturbance versus information gain: Uncertainty relations for quantum information,” *Physical Review A* **53**, 2038 (1996).
- [106] William K Wootters and Wojciech H Zurek, “A single quantum cannot be cloned,” *Nature* **299**, 802–803 (1982).
- [107] Wolfgang Dür, H-J Briegel, Juan Ignacio Cirac, and Peter Zoller, “Quantum repeaters based on entanglement purification,” *Physical Review A* **59**, 169 (1999).
- [108] Yuan Zhan, Paul Hilaire, Edwin Barnes, Sophia E Economou, and Shuo Sun, “Performance analysis of quantum repeaters enabled by deterministically generated photonic graph states,” *Quantum* **7**, 924 (2023).
- [109] Sumeet Khatri, Corey T Matyas, Aliza U Siddiqui, and Jonathan P Dowling, “Practical figures of merit and thresholds for entanglement distribution in quantum networks,” *Physical Review Research* **1**, 023032 (2019).
- [110] Evgeny Shchukin and Peter van Loock, “Optimal Entanglement Swapping in Quantum Repeaters,” *Physical Review Letters* **128**, 150502 (2022).
- [111] Yuan-Mei Xie, Yu-Shuo Lu, Chen-Xun Weng, Xiao-Yu Cao, Zhao-Ying Jia, Yu Bao, Yang Wang, Yao Fu, Hua-Lei Yin, and Zeng-Bing Chen, “Breaking the rate-loss bound of quantum key distribution with asynchronous two-photon interference,” *PRX Quantum* **3**, 020315 (2022).
- [112] Karol Horodecki, Marek Winczewski, and Siddhartha Das, “Fundamental limitations on the device-independent quantum conference key agreement,” *Physical Review A* **105**, 022604 (2022).
- [113] Chen-Long Li, Yao Fu, Wen-Bo Liu, Yuan-Mei Xie, Bing-Hong Li, Min-Gang Zhou, Hua-Lei Yin, and Zeng-Bing Chen, “Breaking the rate-distance limitation of measurement-device-independent quantum secret sharing,” *Physical Review Research* **5**, 033077 (2023).
- [114] Lars Kamin, Evgeny Shchukin, Frank Schmidt, and Peter van Loock, “Exact rate analysis for quantum repeaters with imperfect memories and entanglement swapping as soon as possible,” *Physical Review Research* **5**, 023086 (2023).
- [115] Chen-Long Li, Yao Fu, Wen-Bo Liu, Yuan-Mei Xie, Bing-Hong Li, Min-Gang Zhou, Hua-Lei Yin, and Zeng-Bing Chen, “Breaking universal limitations on quantum conference key agreement without quantum memory,” (2022), arXiv:2212.05226.
- [116] Marek Żukowski, Anton Zeilinger, Michael A Horne, and Arthur K Ekert, “‘‘ event-ready-detectors’’ Bell experiment via entanglement swapping,” *Physical Review Letters* **71** (1993).
- [117] Jian-Wei Pan, Dik Bouwmeester, Harald Weinfurter, and Anton Zeilinger, “Experimental Entanglement Swapping: Entangling Photons That Never Interacted,” *Physical Review Letters* **80**, 3891–3894 (1998).
- [118] S. Bose, V. Vedral, and P. L. Knight, “Multiparticle generalization of entanglement swapping,” *Physical Review A* **57**, 822–829 (1998).
- [119] Aditi Sen(De), Ujjwal Sen, Časlav Brukner, Vladimír Bužek, and Marek Żukowski, “Entanglement swapping of noisy states: A kind of superadditivity in nonclassicality,” *Physical Review A* **72**, 042310 (2005).
- [120] David Deutsch, Artur Ekert, Richard Jozsa, Chiara Macchiavello, Sandu Popescu, and Anna Sanpera, “Quantum privacy amplification and the security of quantum cryptography over noisy channels,” *Physical Review Letters* **77**, 2818 (1996).
- [121] S. Bose, V. Vedral, and P. L. Knight, “Purification via entanglement swapping and conserved entanglement,” *Physical Review A* **60**, 194–197 (1999).

- [122] Xingyu Wang, Chen Dong, Tianyi Wu, Kai Li, Boyu Deng, Lei Shi, and Shanghong Zhao, “Exploiting potentialities for space-based quantum communication network: satellite quantum modelling & downlink scheduling analysis,” (2021), arXiv:2106.00987.
- [123] Markus Aspelmeyer, Thomas Jennewein, Martin Pfenigbauer, Walter R Leeb, and Anton Zeilinger, “Long-distance quantum communication with entangled photons using satellites,” *IEEE Journal of Selected Topics in Quantum Electronics* **9**, 1541–1551 (2003).
- [124] Robert Bedington, Juan Miguel Arrazola, and Alexander Ling, “Progress in satellite quantum key distribution,” *npj Quantum Information* **3**, 30 (2017).
- [125] Cezary Śliwa and Konrad Banaszek, “Conditional preparation of maximal polarization entanglement,” *Physical Review A* **67**, 030101 (2003).
- [126] Koji Azuma, Stefan Bäuml, Tim Coopmans, David Elkouss, and Boxi Li, “Tools for quantum network design,” *AVS Quantum Science* **3** (2021).
- [127] Julian M Bopp, Matthias Plock, Tim Turan, Gregor Pieplow, Sven Burger, and Tim Schröder, “sawfish’ photonic Crystal Cavity for Near-Unity Emitter-to-Fiber Interfacing in Quantum Network Applications,” (2022), arXiv:2210.04702.
- [128] Xiang You, Ming-Yang Zheng, Si Chen, Run-Ze Liu, Jian Qin, Mo-Chi Xu, Zheng-Xuan Ge, Tung-Hsun Chung, Yu-Kun Qiao, Yang-Fan Jiang, Han-Sen Zhong, Ming-Cheng Chen, Hui Wang, Yu-Ming He, Xiu-Ping Xie, Hao Li, Li-Xing You, Christian Schneider, Juan Yin, Teng-Yun Chen, Mohamed Benyoucef, Yong-Heng Huo, Sven Höfling, Qiang Zhang, Chao-Yang Lu, and Jian-Wei Pan, “Quantum interference with independent single-photon sources over 300 km fiber,” *Advanced Photonics* **4**, 066003 (2022).
- [129] Charles H Bennett, François Bessette, Gilles Brassard, Louis Salvail, and John Smolin, “Experimental quantum cryptography,” *Journal of cryptology* **5**, 3–28 (1992).
- [130] Valerio Scarani and Renato Renner, “Quantum Cryptography with Finite Resources: Unconditional Security Bound for Discrete-Variable Protocols with One-Way Postprocessing,” *Physical Review Letters* **100**, 200501 (2008).
- [131] Raymond YQ Cai and Valerio Scarani, “Finite-key analysis for practical implementations of quantum key distribution,” *New Journal of Physics* **11**, 045024 (2009).
- [132] David Pearson, “High-speed QKD reconciliation using forward error correction,” in *AIP Conference Proceedings*, Vol. 734 (American Institute of Physics, 2004) pp. 299–302.
- [133] Juan Yin, Yu-Huai Li, Sheng-Kai Liao, Meng Yang, Yuan Cao, Liang Zhang, Ji-Gang Ren, Wen-Qi Cai, Wei-Yue Liu, Shuang-Lin Li, Rong Shu, Yong-Mei Huang, Lei Deng, Li Li, Qiang Zhang, Nai-Le Liu, Yu-Ao Chen, Chao-Yang Lu, Xiang-Bin Wang, Feihu Xu, Jian-Yu Wang, Cheng-Zhi Peng, Artur K. Ekert, and Jian-Wei Pan, “Entanglement-based secure quantum cryptography over 1,120 kilometres,” *Nature* **582**, 501–505 (2020).
- [134] Douglas B. West, *Introduction to Graph Theory - Second edition* (Pearson, 2000).
- [135] William Thomas Tutte, *Graph theory*, Vol. 21 (Cambridge university press, 2001).
- [136] John A Barnes and Frank Harary, “Graph theory in network analysis,” *Social networks* **5**, 235–244 (1983).
- [137] S. R. Broadbent and J. M. Hammersley, “Percolation processes: I. crystals and mazes,” *Mathematical Proceedings of the Cambridge Philosophical Society* **53**, 629–641 (1957).
- [138] Dietrich Stauffer and Ammon Aharony, *Introduction to percolation theory* (CRC press, 2018).
- [139] Google Quantum AI, “Quantum Computer Datasheet,” <https://quantumai.google/hardware/datasheet/weber.pdf> (2021).
- [140] IBM Quantum (2022), “ibm_washington,” <https://quantum-computing.ibm.com/services/resources> (2022).
- [141] Tomislav Begušić, Johnnie Gray, and Garnet Kin-Lic Chan, “Fast and converged classical simulations of evidence for the utility of quantum computing before fault tolerance,” (2023), arXiv:2308.05077.
- [142] Rigetti Computing, “Aspen-m-2 quantum processor,” <https://qcs.rigetti.com/qpus> (2020).
- [143] Monika Maciag-Kruszewska and ibmblogs, “Polish PSNC to Join IBM Quantum Network, Becoming First Hub in Central and Eastern Europe,” <https://www.ibm.com/blogs/southeast-europe/poland-psnc-ibm-quantum-hub/>.
- [144] Pritam Halder, Ratul Banerjee, Srijon Ghosh, Amit Kumar Pal, and Aditi Sen(De), “Circulating genuine multiparty entanglement in a quantum network,” *Physical Review A* **106**, 032604 (2022).
- [145] Álvaro G Iñesta, Gayane Vardoyan, Lara Scavuzzo, and Stephanie Wehner, “Optimal entanglement distribution policies in homogeneous repeater chains with cutoffs,” *npj Quantum Information* **9**, 46 (2023).
- [146] Luís Bugalho, Bruno C Coutinho, Francisco A Monteiro, and Yasser Omar, “Distributing multipartite entanglement over noisy quantum networks,” *Quantum* **7**, 920 (2023).
- [147] Sumeet Khatri, “Policies for elementary links in a quantum network,” *Quantum* **5**, 537 (2021).
- [148] Yuan Lee, Eric Bersin, Axel Dahlberg, Stephanie Wehner, and Dirk Englund, “A quantum router architecture for high-fidelity entanglement flows in quantum networks,” *npj Quantum Information* **8**, 75 (2022).
- [149] Michał Horodecki and Paweł Horodecki, “Reduction criterion of separability and limits for a class of distillation protocols,” *Physical Review A* **59**, 4206–4216 (1999).
- [150] Reinhard F Werner, “Quantum states with Einstein-Podolsky-Rosen correlations admitting a hidden-variable model,” *Physical Review A* **40**, 4277 (1989).
- [151] Charles Eric Leiserson, Ronald L Rivest, Thomas H Cormen, and Clifford Stein, *Introduction to Algorithms - Third edition* (MIT press Cambridge, MA, USA, 2009).
- [152] Charles H. Bennett, Gilles Brassard, and N. David Mermin, “Quantum cryptography without Bell’s theorem,” *Physical Review Letters* **68**, 557–559 (1992).
- [153] Stefan Bäuml, Matthias Christandl, Karol Horodecki, and Andreas Winter, “Limitations on quantum key repeaters,” *Nature communications* **6**, 6908 (2015).
- [154] Nicolas Sangouard, Christoph Simon, Hugues De Riedmatten, and Nicolas Gisin, “Quantum repeaters based on atomic ensembles and linear optics,” *Reviews of Modern Physics* **83**, 33 (2011).

- [155] Joseph F Fitzsimons, “Private quantum computation: an introduction to blind quantum computing and related protocols,” *npj Quantum Information* **3**, 23 (2017).
- [156] Matthias Steffen, Jay M Gambetta, and Jerry M Chow, “Progress, status, and prospects of superconducting qubits for quantum computing,” in *2016 46th European Solid-State Device Research Conference (ESSDERC)* (IEEE, 2016) pp. 17–20.
- [157] Michał Horodecki, Paweł Horodecki, and Ryszard Horodecki, “Mixed-state entanglement and distillation: Is there a “bound” entanglement in nature?” *Physical Review Letters* **80**, 5239 (1998).
- [158] Karol Horodecki, Michał Horodecki, Paweł Horodecki, and Jonathan Oppenheim, “General paradigm for distilling classical key from quantum states,” *IEEE Transactions on Information Theory* **55**, 1898–1929 (2009).
- [159] René Schwonnek, Koon Tong Goh, Ignatius W Primaatmaja, Ernest Y-Z Tan, Ramona Wolf, Valerio Scarani, and Charles C-W Lim, “Device-independent quantum key distribution with random key basis,” *Nature Communications* **12**, 1–8 (2021).
- [160] Máté Farkas, Maria Balanzó-Juandó, Karol Lukanowski, Jan Kołodyński, and Antonio Acín, “Bell nonlocality is not sufficient for the security of standard device-independent quantum key distribution protocols,” *Physical Review Letters* **127**, 050503 (2021).
- [161] Marek Winczewski, Tamoghna Das, and Karol Horodecki, “Limitations on a device-independent key secure against a nonsignaling adversary via squashed nonlocality,” *Physical Review A* **106**, 052612 (2022).
- [162] Hugo Duminil-Copin, “Introduction to bernoulli percolation,” (2018).
- [163] Michał Horodecki, Paweł Horodecki, and Ryszard Horodecki, “General teleportation channel, singlet fraction, and quasidistillation,” *Physical Review A* **60**, 1888–1898 (1999).
- [164] David Press, Stephan Götzinger, Stephan Reitzenstein, Carolin Hofmann, Andreas Löffler, Martin Kamp, Alfred Forchel, and Yoshihisa Yamamoto, “Photon antibunching from a single quantum-dot-microcavity system in the strong coupling regime,” *Physical Review Letters* **98**, 117402 (2007).
- [165] HG Barros, A Stute, TE Northup, C Russo, PO Schmidt, and R Blatt, “Deterministic single-photon source from a single ion,” *New Journal of Physics* **11**, 103004 (2009).
- [166] Joseph B Altepeter, Evan R Jeffrey, and Paul G Kwiat, “Phase-compensated ultra-bright source of entangled photons,” *Optics Express* **13**, 8951–8959 (2005).
- [167] Charles H. Bennett, David P. DiVincenzo, and John A. Smolin, “Capacities of quantum erasure channels,” *Physical Review Letters* **78**, 3217–3220 (1997).
- [168] K Goodenough, D Elkouss, and S Wehner, “Assessing the performance of quantum repeaters for all phase-insensitive gaussian bosonic channels,” *New Journal of Physics* **18**, 063005 (2016).
- [169] Stefano Pirandola, Riccardo Laurenza, Carlo Ottaviani, and Leonardo Banchi, “Fundamental limits of repeaterless quantum communications,” *Nature Communications* **8**, 15043 (2017).
- [170] Mark M. Wilde, Marco Tomamichel, and Mario Berta, “Converse bounds for private communication over quantum channels,” *IEEE Transactions on Information Theory* **63**, 1792–1817 (2017), arXiv:1602.08898.
- [171] Xiang-Bin Wang, Zong-Wen Yu, and Xiao-Long Hu, “Twin-field quantum key distribution with large misalignment error,” *Physical Review A* **98**, 062323 (2018).
- [172] Xiongfeng Ma, Pei Zeng, and Hongyi Zhou, “Phase-matching quantum key distribution,” *Physical Review X* **8**, 031043 (2018).
- [173] Pei Zeng, Weijie Wu, and Xiongfeng Ma, “Symmetry-protected privacy: beating the rate-distance linear bound over a noisy channel,” *Physical Review Applied* **13**, 064013 (2020).
- [174] Yuan-Mei Xie, Chen-Xun Weng, Yu-Shuo Lu, Yao Fu, Yang Wang, Hua-Lei Yin, and Zeng-Bing Chen, “Scalable high-rate twin-field quantum key distribution networks without constraint of probability and intensity,” *Physical Review A* **107**, 042603 (2023).
- [175] Lai Zhou, Jinping Lin, Yuan-Mei Xie, Yu-Shuo Lu, Yumang Jing, Hua-Lei Yin, and Zhiliang Yuan, “Experimental Quantum Communication Overcomes the Rate-Loss Limit without Global Phase Tracking,” *Physical Review Letters* **130**, 250801 (2023).
- [176] Réka Albert, Hawoong Jeong, and Albert-László Barabási, “Error and attack tolerance of complex networks,” *Nature* **406**, 378–382 (2000).
- [177] Duncan S Callaway, Mark EJ Newman, Steven H Strogatz, and Duncan J Watts, “Network robustness and fragility: Percolation on random graphs,” *Physical Review Letters* **85**, 5468 (2000).
- [178] Arman Mohseni-Kabir, Mihir Pant, Don Towsley, Saikat Guha, and Ananthram Swami, “Percolation thresholds for robust network connectivity,” *Journal of Statistical Mechanics: Theory and Experiment* **2021**, 013212 (2021).
- [179] Linton C Freeman, Douglas Roeder, and Robert R Mulholland, “Centrality in social networks: II. Experimental results,” *Social networks* **2**, 119–141 (1979).
- [180] Linton C Freeman, “A set of measures of centrality based on betweenness,” *Sociometry* , 35–41 (1977).
- [181] Corrado Gini, “Variabilità e mutabilità (Variability and Mutability),” *C. Cuppini, Bologna* , 156 (1912).
- [182] William Stallings, “Local networks,” *ACM Computing Surveys (CSUR)* **16**, 3–41 (1984).
- [183] P Green, “An introduction to network architectures and protocols,” *IEEE Transactions on Communications* **28**, 413–424 (1980).
- [184] Duncan J Watts and Steven H Strogatz, “Collective dynamics of ‘small-world’ networks,” *Nature* **393**, 440–442 (1998).
- [185] Google, “*Satellite network*,” ([Online]).
- [186] Stefanie Barz, Elham Kashefi, Anne Broadbent, Joseph F Fitzsimons, Anton Zeilinger, and Philip Walther, “Demonstration of blind quantum computing,” *science* **335**, 303–308 (2012).
- [187] Anton Zeilinger, Michael A. Horne, Harald Weinfurter, and Marek Żukowski, “Three-Particle Entanglements from Two Entangled Pairs,” *Physical Review Letters* **78**, 3031–3034 (1997).
- [188] Sébastien de Bone, Runsheng Ouyang, Kenneth Goodenough, and David Elkouss, “Protocols for creating and distilling multipartite GHZ states with Bell pairs,” *IEEE Transactions on Quantum Engineering* **1**, 1–10 (2020).

- [189] Paul Nation, Hanhee Paik, Andrew Cross, and Zaira Nazario, “The IBM Quantum heavy hex lattice,” <https://research.ibm.com/blog/heavy-hex-lattice> (2021).
- [190] Kelvin Lawrence, “Air route data - and more!” ([Online]).
- [191] U.S. Department of Energy Office of Science, “National QIS research centers,” <https://science.osti.gov/-/media/QIS/pdf/QuantumBrochure2021.pdf>.
- [192] Eddie Schoute, Laura Mancinska, Tanvirul Islam, Iordanis Kerenidis, and Stephanie Wehner, “Shortcuts to quantum network routing,” (2016), arXiv:1610.05238.
- [193] Edsger W Dijkstra, “A note on two problems in connexion with graphs,” *Numerische Mathematik* **1**, 269–271 (1959).
- [194] Charles H Bennett, David P DiVincenzo, John A Smolin, and William K Wootters, “Mixed-state entanglement and quantum error correction,” *Physical Review A* **54**, 3824 (1996).
- [195] Karl Kraus, “General state changes in quantum theory,” *Annals of Physics* **64**, 311–335 (1971).
- [196] Man-Duen Choi, “Completely positive linear maps on complex matrices,” *Linear Algebra and Its Applications* **10**, 285–290 (1975).
- [197] KM Fonseca Romero and R Lo Franco, “Simple non-markovian microscopic models for the depolarizing channel of a single qubit,” *Physica Scripta* **86**, 065004 (2012).
- [198] Markus Grassl, Th Beth, and Thomas Pellizzari, “Codes for the quantum erasure channel,” *Physical Review A* **56**, 33 (1997).
- [199] D Vasylyev, AA Semenov, and W Vogel, “Atmospheric quantum channels with weak and strong turbulence,” *Physical Review Letters* **117**, 090501 (2016).
- [200] Federico Dios, Juan Antonio Rubio, Alejandro Rodríguez, and Adolfo Comerón, “Scintillation and beam-wander analysis in an optical ground station-satellite uplink,” *Applied Optics* **43**, 3866–3873 (2004).
- [201] Morio Toyoshima and Kenichi Araki, “Far-field pattern measurement of an onboard laser transmitter by use of a space-to-ground optical link,” *Applied Optics* **37**, 1720–1730 (1998).
- [202] Sebastian KH Andersen, Shailesh Kumar, and Sergey I Bozhevolnyi, “Ultrabright linearly polarized photon generation from a nitrogen vacancy center in a nanocube dimer antenna,” *Nano Letters* **17**, 3889–3895 (2017).
- [203] Brian J Smith, P Mahou, Offir Cohen, JS Lundeen, and IA Walmsley, “Photon pair generation in birefringent optical fibers,” *Optics Express* **17**, 23589–23602 (2009).
- [204] Matthias J Bayerbach, Simone E D’Aurelio, Peter van Loock, and Stefanie Barz, “Bell-state measurement exceeding 50% success probability with linear optics,” (2022), arXiv:2208.02271.
- [205] Ryszard Horodecki, Pawel Horodecki, and Michal Horodecki, “Violating Bell inequality by mixed spin-12 states: necessary and sufficient condition,” *Physics Letters A* **200**, 340–344 (1995).
- [206] William K Wootters, “Entanglement of formation of an arbitrary state of two qubits,” *Physical Review Letters* **80**, 2245 (1998).